Roots branch towards water by post-translational modification of transcription factor ARF7

Beatriz Orosa-Puente[1,9†], Nicola Leftley[2†], Daniel von Wangenheim[2†], Jason Banda[2], Anjil K Srivastava[1], Kristine Hill[2,10], Jekaterina Truskina[2,3], Rahul Bhosale[2], Emily Morris[2], Moumita Srivastava[1] Britta Kümpers[2], Tatsuaki Goh[2,4,11], Hidehiro Fukaki[4], Joop EM Vermeer[5,6], Teva Vernoux[3], José R. Dinneny[7], Andrew P. French[2,8], Anthony Bishopp[2], Ari Sadanandom[1*] & Malcolm J. Bennett[2*]

[1]*Department of Biosciences, University of Durham, Durham, DH1 3LE, UK.*

[2]*Plant & Crop Sciences, School of Biosciences, University of Nottingham, LE12 5RD, UK.*

[3]*Laboratoire Reproduction et Developpement des Plantes, Univ Lyon, ENS de Lyon, F-69342, Lyon, France*

[4] *Department of Biology, Graduate School of Science, Kobe University, Kobe 657-8501, Japan*
[5]*Department of Plant and Microbial Biology, University of Zurich, CH-8008 Zurich, Switzerland*
[6]*Developmental Biology, Wageningen University and Research, Wageningen, the Netherlands*
[7]*Department of Biology, Stanford University, Stanford, CA 94305, USA*
[8]*School of Computer Science, Jubilee Campus, University of Nottingham, NG8 1BB, UK.*

[9]*New address: School of Biological Sciences, University of Edinburgh, EH9 3FF, UK.9*

[10]*New address: Center for Plant Molecular Biology – ZMBP, University of Tübingen, D - 72076 Tübingen, Germany*

[11]*New address: Graduate School of Science and Technology, Nara Institute of Science and Technology, 8916-5 Takayama, Ikoma 630-0192, Japan*

[†]These authors have contributed equally

[†]Beatriz Orosa-Puente ORCID ID: 0000-0003-0362-4532
[†]Nicola Leftley ORCID ID: 0000-0001-5795-0822
[†]Daniel von Wangenheim ORCID ID: 0000-0002-6862-1247

[*]Joint corresponding authors

Professor Ari Sadanandom
Email: ari.sadanandom@durham.ac.uk; FON +44 191 33 41263
ORCID ID: 0000-0003-0058-9479

Professor Malcolm J. Bennett
Email: Malcolm.bennett@nottingham.ac.uk ; FON +44 115 951 3255
ORCID ID: 0000-0003-0475-390X

Abstract:

Plants adapt to heterogeneous soil conditions by altering their root architecture. For example, roots branch when in contact with water using the hydropatterning response. We report that hydropatterning is dependent on auxin response factor ARF7. This transcription factor induces asymmetric expression of its target gene *LBD16* in lateral root founder cells on the side of the root in contact with water. This differential expression pattern is regulated by post-translational modification of ARF7 with the SUMO protein. SUMOylation negatively regulates ARF7 DNA binding activity. ARF7 SUMOylation is required to recruit the Aux/IAA repressor protein IAA3. Blocking ARF7 SUMOylation disrupts IAA3 recruitment and hydropatterning. We conclude that SUMO-dependent regulation of auxin response controls root branching pattern in response to water availability.

119 words

One Sentence Summary:

Auxin hormone signaling links root branching with water availability.

69 characters

The soil resources plants require like water are often distributed heterogeneously (*1*). To aid foraging, root development is responsive to the spatial availability of soil signals (*2, 3*). MicroCT imaging revealed soil-water contact impacts root architecture, causing lateral roots to form when roots are in direct contact with moisture (*4, 5*). This adaptive branching response is termed hydropatterning (*4, 5*). In this current study we report the molecular mechanism controlling hydropatterning, revealing core components of the auxin response machinery are targets for post-translational regulation.

The hydropatterning response can be mimicked *in vitro* by growing seedling roots vertically on the surface of agar plates (Fig. 1A)(*4*). Opposite sides of a root are either in contact with moisture (directly with the plate or via the meniscus) or exposed to air (Fig. S1). To visualize whether primordia preferentially form on the side in contact with moisture, we transferred a root including the gel it was growing on, into a Light Sheet Fluorescence Microscope to image young primordia and measure their angle of outgrowth with respect to the agar surface (Fig. S1). This revealed lateral roots preferentially emerge from the side of the root in contact with moisture (Fig. 1A).

What causes new primordia to form on the water-contact side of a root? Seedlings exposed to a hydropatterning stimulus exhibit an auxin response gradient across the root radius (*4*). Auxin regulates lateral root development (*6*). Auxin responsive gene expression is regulated by a family of transcription factors termed auxin response factors (ARF) (*7*). The model plant *Arabidopsis thaliana* contains five *ARF* transcriptional activating genes termed *ARF5, 6, 7, 8* and *19* (*8*). To determine which ARF gene(s) controls hydropatterning, we phenotyped loss of function alleles. ARF7 mutants (*8*, *9*) were all impaired (Fig. 1A,B, C & S2), whereas

hydropatterning was normal in mutants of other ARF family members tested (Fig. S3). Hence, hydropatterning appears ARF7 dependent.

ARF7 regulates lateral root initiation (*8*, *10*, *11* reviewed in *6*). Network inference, ChIP-PCR validation and transcriptomic studies have revealed that ARF7 controls the auxin-dependent expression of lateral root regulatory genes such as *LBD16* (Fig. S4)(*12*). Like *ARF7*, *LBD16* loss of function alleles *lbd16-1* and *lbd16-2* exhibit a hydropatterning defect (Fig. S5). ARF7 may therefore control hydropatterning in an *LBD16*-dependent manner. *LBD*-like genes are differentially expressed in maize during hydropatterning (5). To determine whether *LBD16* is differentially expressed in response to a hydropatterning stimulus by ARF7, we monitored spatial expression of a *gLBD16-GFP* reporter (*13*). LBD16-GFP was first detected in the elongation zone (Fig. 1D; Movie S1) in a subset of cells (termed xylem pole pericycle [XPP] founder cells from which primordia originate), consistent with this reporter being an early marker for lateral root development (*13*). In Arabidopsis lateral roots originate from pericycle cells positioned above either xylem pole (*6*). We tested whether *gLBD16-GFP* was differentially expressed in XPP cell files closest to the agar. To mark which side of a root was exposed to air, we overlaid samples with low melting point agar containing fluorescent beads, then imaged from multiple angles employing light-sheet microscopy (Fig. S6-8). Reconstructed root images revealed preferential *gLBD16-GFP* expression in XPP cell nuclei earlier on one side of WT roots (Fig. 1E). Asymmetric *gLBD16-GFP* expression was disrupted in *arf7-1* (Fig. 1E, F), consistent with the mutant's hydropatterning defect (Fig. 1C). Quantification of *LBD16-GFP* distribution in WT and *arf7-1* revealed this reporter was differentially expressed in an ARF7-dependent manner (Fig. S8A-D, F). To test whether asymmetric *LBD16* expression is essential for hydropatterning,

the constitutive 35S promoter was used to drive *LBD16* expression in *lbd16* (Fig. S9). *35S:LBD16* expression failed to rescue the *lbd16* hydropatterning defect (in contrast to *LBD16:LBD16-GFP*). Hence, asymmetric *LBD16* expression is essential for hydropatterning.

We next tested whether LBD16-dependent hydropatterning was controlled via differential ARF7 expression using transcriptional and translational *ARF7pro::ARF7-VENUS* reporters (Fig. S10, S11). In contrast to *gLBD16-GFP* (Fig. 1E, F), ARF7 reporters did not exhibit differential expression in LR stem cells (Fig. 1G). To test whether ARF7 was a target of post-translational regulation, ARF7 was constitutively expressed (using the 35S promoter) in *arf7-1*. This revealed *35S:ARF7* could rescue *arf7-1* hydropatterning (Fig. 1C, S12). Hence, ARF7 appears to control hydropatterning via a post-translational (rather than transcriptional) mechanism.

ARF7 contains post-translational regulatory motifs including 4 putative sites for addition of Small Ubiquitin MOdifier (SUMO) proteins at lysine residues (K104, K151, K282 and K889) (Fig. 2A). SUMO, unlike ubiquitin, can modify the function (rather than abundance) of target proteins (*14*). We confirmed ARF7 is a target for SUMOylation by co-expressing GFP and HA tagged ARF7 and SUMO sequences (Fig. 2B). Addition of SUMO to ARF7 is abolished after replacing lysine for arginine in all four ARF7 SUMOylation motifs (in *gARF7-*$^{4K/R}$; Fig. 2B).

To test the importance of ARF7 SUMOylation for LR development and hydropatterning, we expressed SUMOylatable gARF7 and non-SUMOylatable *gARF7-*$^{4K/R}$ transgenes in *arf7-1*. Bioassays revealed *arf7* hydropatterning could be rescued by wild type *gARF7* (Fig. 2C, D, S13) but not by *gARF7-*$^{4K/R}$ (Fig. 2E, F, S14). Nevertheless, *gARF7-*$^{4K/R}$ (like *gARF7*) remained capable of restoring *arf7* lateral root density to a WT level (Fig. 2F). Hence, ARF7-$^{4K/R}$ remained

functional, but unable to regulate hydropatterning. Quantification of *LBD16-GFP* distribution in *gARF7* versus *gARF7-$^{4K/R}$ arf7-1* revealed this reporter was only differentially expressed in the presence of SUMOylatable ARF7 (Fig. S8A-C, E, G). We conclude ARF7 SUMOylation is required for hydropatterning.

How does SUMOylation modify ARF7 activity? ARF7 is rapidly SUMOylated following auxin treatment (Fig. 2G). One ARF7 SUMOylation site (K151) is located within the DNA binding domain (Fig. 2A)(*15*). SUMOylation may attenuate auxin-induced ARF7 DNA binding activity. Time course ChIP-PCR analysis revealed ARF7 transiently interacts with the *LBD16* promoter following auxin treatment (Fig. S15). Furthermore, ChIP-PCR assays performed on *LBD16* and *LBD29* target promoters detected higher DNA binding by ARF7-$^{4K/R}$-GFP than WT ARF7-GFP (Fig. S16). Hence, SUMOylation negatively regulates ARF7 DNA binding activity.

ARF7 transcriptional activity is negatively regulated by Aux/IAA repressor proteins (*16*). Aux/IAAs such as IAA3/SHY2 and IAA14/SLR control ARF7 activity during LR development (*16*, *17*). Like *arf7-1*, *IAA3* loss of function allele *shy2-31* causes a LR hydropatterning defect (Fig. 3A, S17). Thus we tested whether interactions between ARF7, IAA3/SHY2 and IAA14/SLR were SUMO dependent. Pull down assays revealed ARF7-GFP interacted with IAA3/SHY2 and IAA14/SLR proteins (Fig. S18). In contrast, non-SUMOylatable ARF7-$^{4K/R}$ largely failed to pull down IAA3/SHY2. However, both forms of ARF7 interacted with IAA14/SLR (Fig. S19). Hence, interaction between ARF7 and IAA3/SHY2 (but not IAA14/SLR) depends on the residues that regulate ARF7 SUMOylation.

Bioinformatic analysis revealed *IAA3/SHY2* (but not *IAA14/SLR*) contained a SUMO interaction motif (SIM) (Fig. 3B). With its SIM domain mutated, interaction between IAA3 and

WT ARF7 was abolished (Fig. 3C). Nevertheless, the IAA3 SIM mutant protein could interact with the TIR1 auxin receptor and TPL transcriptional repressor (Fig. S19, S20). Hence, mutating the SIM site differentially affects IAA3's ability to interact with SUMOylated ARF7, but not other partners.

To assess the functional importance of the *IAA3* SIM sequence *in planta*, we engineered transgenic plants overexpressing *shy2-2* with or without SIM sequences. We examined the impact of the SIM sequence on the suppression of root branching characteristic of *shy2-2* mutant plants *(18),* a phenotype not dependent on hydropatterning. We drove overexpression of the *shy2-2* gene with the endodermal-specific CASP promoter. More root branching is evident in roots of plants expressing p*CASP:shy2-2* without the SIM sequence than in plants expressing p*CASP:shy2-2* with the SIM sequence (Fig. 3D). Thus overexpression of shy2-2 in endodermis can block ARF7-dependent lateral root development, but only if the SIM sequence is included.

SUMO modifiers are added and removed from target roteins by E3 ligases and SUMO proteases, respectively. In *Arabidopsis*, OTS1 and OTS2 proteases cleave off SUMO from nuclear localized proteins (*19*). Pull down assays revealed ARF7 is a direct target for OTS1 (Fig. S21). Our bioassays revealed the *ots1 ots2* mutant exhibits a hydropatterning defect (Fig. S22). Hence, hydropatterning appears dependent on OTS1 and OTS2 function. These SUMO proteases are labile when plants are exposed to abiotic stress, causing their SUMOylated target proteins to accumulate (*19*, *20*). Indeed, transiently exposing *gARF7-GFP* seedlings to 20 minutes outside an agar plate resulted in a rapid increase in ARF7 SUMOylation (Fig. 2H). Hence, it is the absence (rather than the presence) of water that stimulates this post-translational response.

Modelling suggests a substantial differential in water potential is generated across the air and contact axis of the root (*5*). We hypothesize this triggers SUMOylated ARF7 on the air side of roots to recruit IAA3 and create a transcriptional repressor complex, thereby blocking auxin responsive gene expression associated with lateral root initiation (Fig. 3E). Conversely, since IAA3 cannot be recruited by non-SUMOylated ARF7 in root cells on the contact side, this population of transcription factors can induce expression of genes like *LBD16* to trigger organ initiation (Fig. 3E).

Our study has revealed how environmental inputs modulate the auxin response machinery. The SUMO-mediated post-translational regulation of auxin signalling operates on top of the specificity provided from distribution of the hormone itself and the expression patterns of individual regulatory components. Thus auxin regulation controls root branching pattern in response to water availability, building a root architecture that optimizes access to water.

~1521 words (main text)

Legends

Fig. 1. Arabidopsis root branching towards water is ARF7 dependent (A, B) Cross section schematic of a root growing on agar. Lateral root primordia outgrowth angle (yellow lines) in respect to the agar surface quantified from 3D light-sheet microscopy images of wildtype (A) and *arf7-1* (B) plants. (C) Hydropatterning bioassay of wildtype (WT), *arf7* and *arf7* overexpressing ARF7 (*p35S::ARF7*). Data shown is mean values ± S. E. Statistical differences were analysed on the percent of emerged LRs emerging towards either contact or air using an Anova, Tukey HSD test ($P<0.05$); statistically similar groups are indicated using the same letter. (D) Confocal image of Arabidopsis root tip expressing *gLBD16-GFP*. Grey boxed area

highlights onset of LBD16-GFP expression in the elongation zone. (E, F, G) Maximum intensity projections of radial re-slices obtained from LSFM-Multiview imaging show the gene expression pattern of LBD16-GFP in wildtype (E) and, *arf7* (F) and *ARF7::ARF7-Venus* (G) on the contact versus air sides. The number under the (E) and (F) displays the index of asymmetry. Positive values correspond to an earlier expression beginning on the contact side, negative values show asymmetry towards the air side. Details explained in Fig. S1, 6-8. Scale bars 50um.

Fig. 2. ARF7 SUMOylation regulates hydropatterning and DNA binding affinity (A) Schematic of ARF7 domains and four predicted SUMO sites K104, K151, K282 and K889. (B) Replacing all ARF7 SUMO site lysine with arginine residues in ARF7-GFP(4*K/R) blocks SUMOylation with HA-SUMO1 (but not WT ARF7 or single SUMO K104) in transient expression assays. (C-D) Bioassays reveal 2 independent transgenic lines expressing WT gARF7 can rescue *arf7-1* hydropatterning (C) and LR density defects (D), n LR=196/78/292/231 n Plants=7/5/10/9. (E-F) Bioassays reveal 3 independent transgenic lines expressing gARF7(4*K/R) cannot rescue *arf7-1* hydropatterning (E) but does restore LR density (F), n LR=374/268/198/286/206 n Plants=12/16/8/11/8. Data is mean values ± S. E. and statistics performed as Fig. 1C. (G) Immunoprecipitation reveals ARF7-GFP [but not ARF7-GFP(4*K/R)] is rapidly SUMOylated 15’ after NAA treatment. (H) Immunoprecipitation reveals ARF7-GFP [but not ARF7-GFP(4*K/R)] is rapidly SUMOylated 20’ after seedlings were removed from their agar plates.

Fig. 3 SHY2 interacts with ARF7 in a SUMO-dependent manner to control hydropatterning

(A) Bioassay reveals *IAA3/SHY2* mutant allele *shy2-31* does not exhibit a hydropatterning response. Data shown is mean ± S. E. Letters indicate a significant difference compared to WT (L*er*) roots based on Student *t* test ($p<0.05$), n LR=208/604 n Plants=7/19. (B) The *IAA3* (but not *IAA14*) sequence contains a putative SUMO-Interaction-Motif (SIM), suggesting IAA3 could bind SUMOylated ARF7. (C) Transient expression of IAA3/SHY2-HA(WT-SIM) or IAA3/SHY2-HA(SIM mutant) with ARF7-GFP or ARF7-

GFP(4*K/R), followed by immunoprecipitation and western analysis, revealed IAA3 interacts with ARF7 in a SIM and SUMO-dependent manner. (D) Phenotyping Arabidopsis seedlings expressing *shy2-2* ± SIM using the endodermal *CASP1* promoter, revealed *CASP1:shy2-2* (WT) blocks LR branching (upper tier) whereas *CASP1:shy2-2* (non-SIM) branch normally (lower tier). Seedlings are from six independent lines termed SIM containing *CASP1:shy2-2* (WT L1, L2 and L3) and non-SIM containing *CASP1:shy2-2* (SIML1, L2 and L3) (E) Schematic summarizing SUMO-dependent ARF7 model for hydropatterning, where on the air side of the root ARF7 is SUMOylated, resulting in an interaction with IAA3 that inhibits LR initiation. On the contact side of the root, ARF7 is not SUMOylated, enabling the transcriptional factor to activate expression of genes involved in LR initiation.

References and Notes:

1. A. Hodge, The plastic plant: root responses to heterogeneous supplies of nutrients. *New Phytol.* **162**, 9–24 (2004).

2. B. D. Gruber, R. F. H. Giehl, S. Friedel, N. von Wirén, Plasticity of the Arabidopsis Root System under Nutrient Deficiencies. *Plant Physiol.* **163**, 161–179 (2013).

3. E. C. Morris *et al.*, Shaping 3D Root System Architecture. *Curr. Biol.* **27** (2017).

4. Y. Bao *et al.*, Plant roots use a patterning mechanism to position lateral root branches toward available water. *Proc. Natl. Acad. Sci. U. S. A.* **111**, 9319–24 (2014).

5. N. E. Robbins, J. R. Dinneny, Growth is required for perception of water availability to pattern root branches in plants. *Proc. Natl. Acad. Sci. U. S. A.* **115**, E822–E831 (2018).

6. J. Lavenus *et al.*, Lateral root development in Arabidopsis: fifty shades of auxin. *Trends Plant Sci.* **18**, 450–458 (2013).

7. T. Ulmasov, J. Murfett, G. Hagen, T. J. Guilfoyle, Aux/IAA proteins repress expression of reporter genes containing natural and highly active synthetic auxin response elements.

Plant Cell. **9**, 1963–71 (1997).

8. Y. Okushima *et al.*, Functional Genomic Analysis of the AUXIN RESPONSE FACTOR Gene Family Members in Arabidopsis thaliana: Unique and Overlapping Functions of ARF7 and ARF19. *Plant Cell*. **17**, 444–463 (2005).

9. R. Harper *et al.*, The NPH4 locus encodes the auxin response factor ARF7, a conditional regulator of differential growth in aerial Arabidopsis tissue. *Plant Cell*. **12**, 757–770 (2000).

10. M. A. Moreno-Risueno *et al.*, Oscillating Gene Expression Determines Competence for Periodic Arabidopsis Root Branching. *Science (80-.).* **329**, 1306–1311 (2010).

11. B. Péret *et al.*, Auxin regulates aquaporin function to facilitate lateral root emergence. *Nat. Cell Biol.* **14**, 991–998 (2012).

12. J. Lavenus *et al.*, Inference of the Arabidopsis Lateral Root Gene Regulatory Network Suggests a Bifurcation Mechanism That Defines Primordia Flanking and Central Zones. *Plant Cell*. **27**, 1368–1388 (2015).

13. T. Goh *et al*., The establishment of asymmetry in *Arabidopsis* lateral root founder cells is regulated by LBD16/ASL18 and related LBD/ASL proteins. *Development*. **139**, 883-93 (2012).

14. E. S. Johnson, Protein Modification by SUMO. *Annu. Rev. Biochem.* **73**, 355–382 (2004).

15. D. R. Boer *et al.*, Structural basis for DNA binding specificity by the auxin-dependent ARF transcription factors. *Cell*. **156**, 577–89 (2014).

16. T. Goh, H. Kasahara, T. Mimura, Y. Kamiya, H. Fukaki, Multiple AUX/IAA-ARF

modules regulate lateral root formation: the role of Arabidopsis SHY2/IAA3-mediated auxin signalling. *Philos. Trans. R. Soc. Lond. B. Biol. Sci.* **367**, 1461–8 (2012).

17. K. Swarup *et al.*, The auxin influx carrier LAX3 promotes lateral root emergence. *Nat. Cell Biol.* **10**, 946–954 (2008).

18. J. E. M. Vermeer *et al.*, A spatial accommodation by neighboring cells is required for organ initiation in arabidopsis. *Science (80-.).* **343** (2014).

19. L. Conti *et al.*, Small Ubiquitin-like Modifier Protein SUMO Enables Plants to Control Growth Independently of the Phytohormone Gibberellin. *Dev. Cell*. **28**, 102–110 (2014).

20. L. Conti *et al.*, Small ubiquitin-like modifier proteases OVERLY TOLERANT TO SALT1 and -2 regulate salt stress responses in Arabidopsis. *Plant Cell*. **20**, 2894–908 (2008).

21. T. Nakagawa *et al.*, Improved Gateway Binary Vectors: High-Performance Vectors for Creation of Fusion Constructs in Transgenic Analysis of Plants, doi:10.1271/bbb.70216.

22. S. J. Clough, A. F. Bent, Floral dip: a simplified method for Agrobacterium-mediated transformation of Arabidopsis thaliana. *Plant J.* **16**, 735–43 (1998).

23. M. M. Goodin, R. G. Dietzgen, D. Schichnes, S. Ruzin, A. O. Jackson, pGD vectors: versatile tools for the expression of green and red fluorescent protein fusions in agroinfiltrated plant leaves. *Plant J.* **31**, 375–383 (2002).

24. J. D. Nelson, O. Denisenko, P. Sova, K. Bomsztyk, Fast chromatin immunoprecipitation assay. *Nucleic Acids Res.* **34**, e2 (2006).

25. H. Cho *et al.*, A secreted peptide acts on BIN2-mediated phosphorylation of ARFs to potentiate auxin response during lateral root development. *Nat. Cell Biol.* **16**, 66–76 (2014).

26. D. von Wangenheim, R. Hauschild, J. Friml, Light sheet fluorescence microscopy of plant roots growing on the surface of a gel. *J. Vis. Exp.* **2017** (2017).

27. S. Preibisch *et al.*, Efficient Bayesian-based multiview deconvolution. *Nat. Methods*. **11**, 645–648 (2014).

28. S. Preibisch, S. Saalfeld, J. Schindelin, P. Tomancak, Software for bead-based registration of selective plane illumination microscopy data. *Nat. Methods*. **7**, 418–419 (2010).

Acknowledgments: We acknowledge Tom Guilfoyle for insightful discussions and dedicate this manuscript in his memory. We thank Jennifer Dewick for assisting submitting this manuscript.

Funding: This work was supported by the awards from the Biotechnology and Biological Sciences Research Council [grant numbers BB/G023972/1, BB/R013748/1, BB/L026848/1, BB/M018431/1, BB/PO16855/1, BB/M001806/1]; European Research Council (ERC) FUTUREROOTS Advanced grant 294729; ERC SUMOrice Consolidator grant 310235; Leverhulme Trust grant RPG-2016-409; ANR 2014-CE11-0018 Serrations grant; AuxID PICS grant from the CNRS; a joint INRA/University of Nottingham PhD grant to J. T.; JEMV is supported by the Swiss National Science Foundation (PP00P3_157524 and 316030_164086) and the Netherlands Organization for Scientific Research (NWO 864.13.008). H.F was supported by a Grant-in-Aid for Scientific Research on Priority Areas (19060006) from the MEXT, Japan.

Author contributions: B.O.P, N.L, D. W, J.B., K.H., H.F., J.E.M.V., T.V., J.D., A.F., A.B., A.S. and M.B. designed experiments; B.O.P, N.L, D. W, J.B, A.K.S., K.H., J.T., R.B., E.M., M.S., B.K. and T.G. performed experiments; and B.O.P, N.L, D.W, A.B., A.S. and M.B. wrote the manuscript. **Competing interests:** “Authors declare no competing interests.” **Data and**

materials availability: No restrictions are placed on materials, such as materials transfer agreements. Details of all data, code and materials used in the analysis are available in the main text or the supplementary materials.

315

Materials and Methods

Figures S1-S18

Tables S1-S2

Movies S1

320 References supplement

(*21*)(*22*)(*23*)(*24*)(*25*)(*26*)(*27*, *28*)

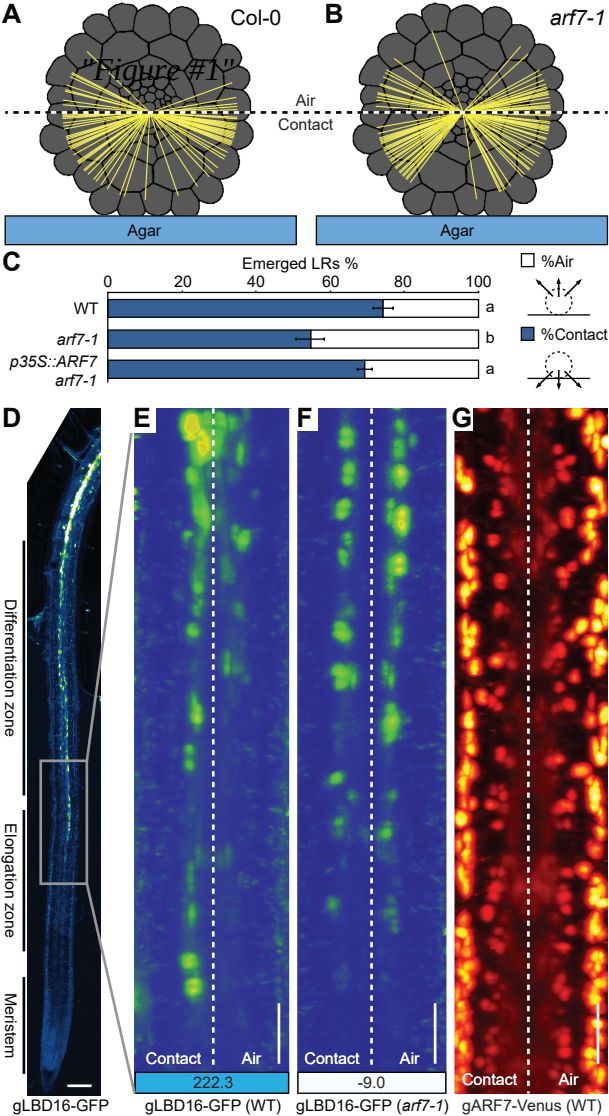
A
Col-0
"Figure #1"
B
arf7-1
Air
Contact
Agar
Agar
C
Emerged LRs %
0
20
40
60
80
100
WT
arf7-1
p35S::ARF7
arf7-1
a
b
a
%Air
%Contact
D
Differentiation zone
Elongation zone
Meristem
E
F
G
Contact
Air
222.3
Contact
Air
-9.0
Contact
Air
gLBD16-GFP
gLBD16-GFP (WT)
gLBD16-GFP (arf7-1)
gARF7-Venus (WT)

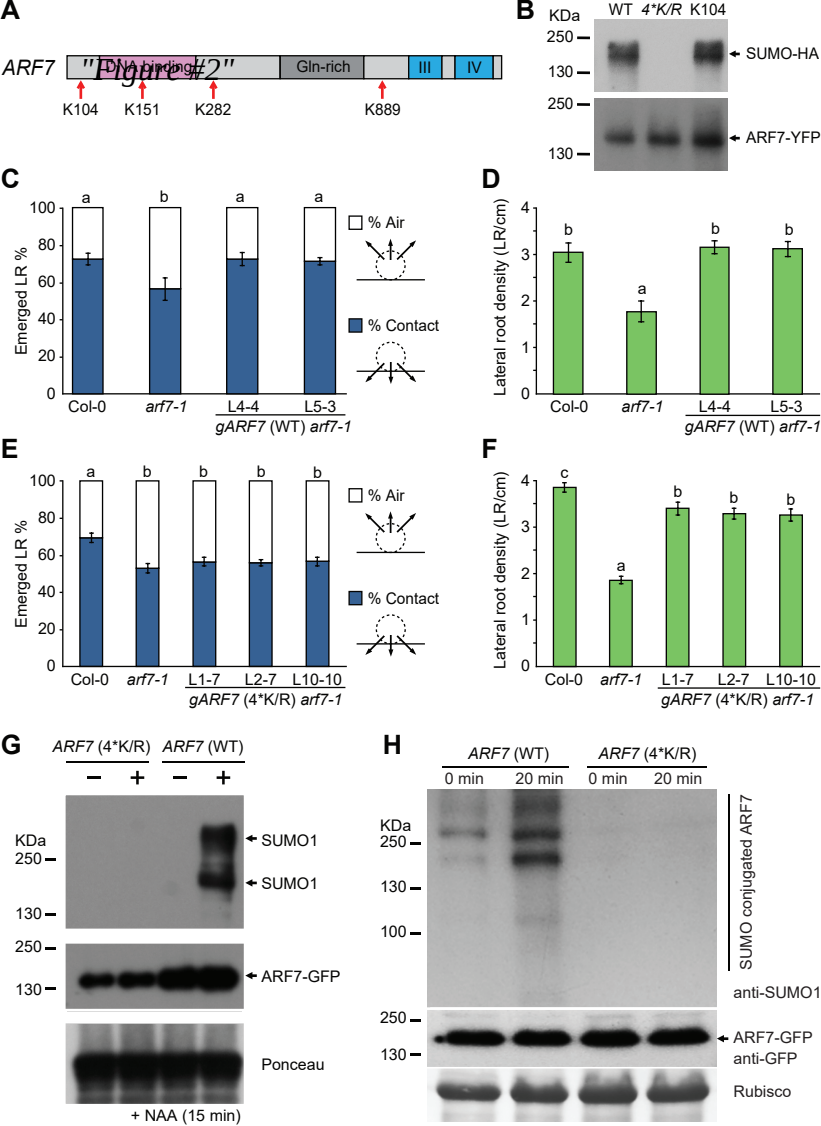
A
ARF7
DNA binding
Gln-rich
III
IV
K104
K151
K282
K889
B
KDa
WT
4*K/R
K104
250
130
SUMO-HA
ARF7-YFP
C
Emerged LR %
% Air
% Contact
Col-0
arf7-1
L4-4
L5-3
gARF7 (WT) arf7-1
D
Lateral root density (LR/cm)
E
L1-7
L2-7
L10-10
gARF7 (4*K/R) arf7-1
F
G
ARF7 (4*K/R)
ARF7 (WT)
SUMO1
ARF7-GFP
Ponceau
+ NAA (15 min)
H
0 min
20 min
SUMO conjugated ARF7
anti-SUMO1
ARF7-GFP
anti-GFP
Rubisco

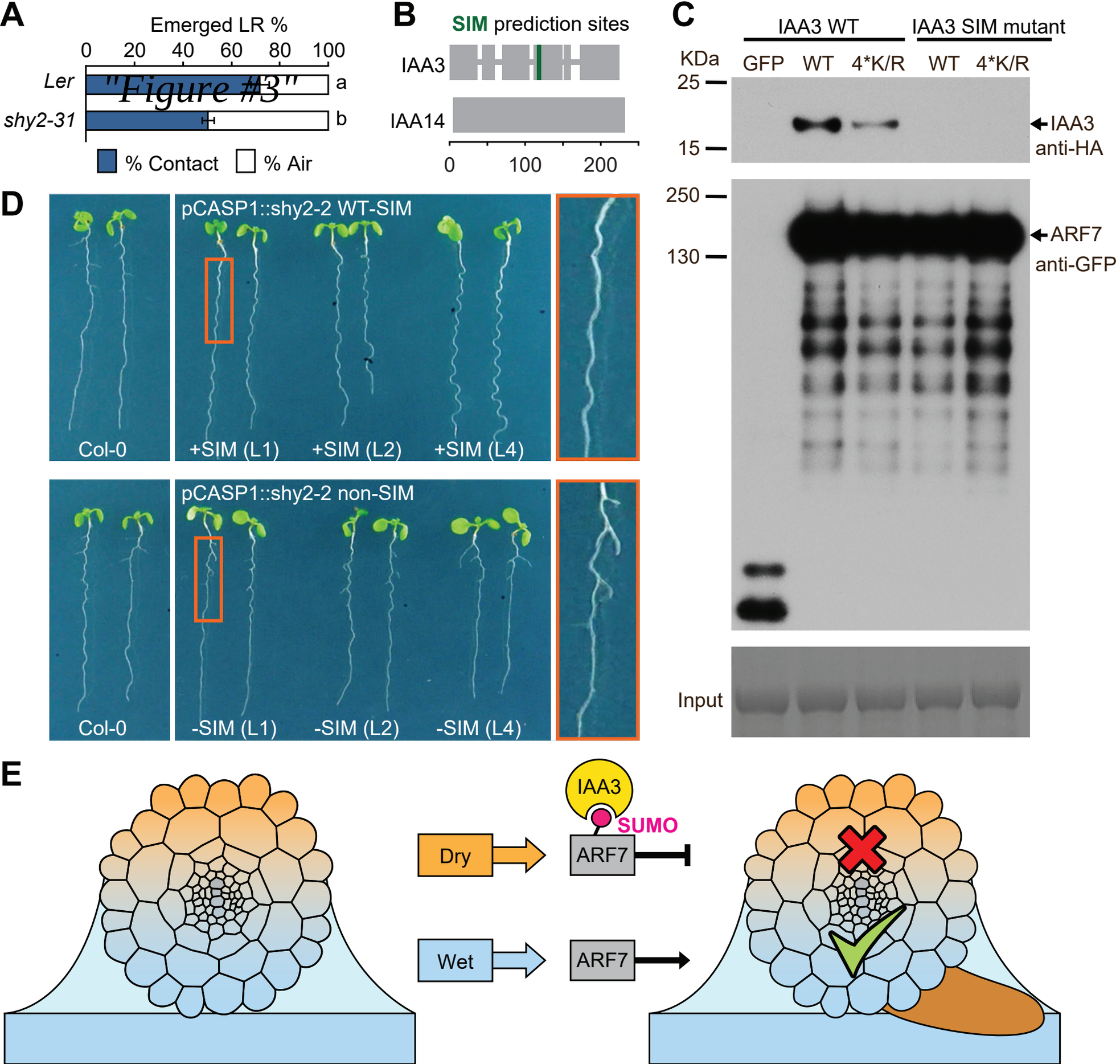
A
Emerged LR %
0 20 40 60 80 100
Ler
shy2-31
a
b
% Contact
% Air
"Figure #3"
B
SIM prediction sites
IAA3
IAA14
0 100 200
C
IAA3 WT
IAA3 SIM mutant
KDa
GFP WT 4*K/R WT 4*K/R
25
15
IAA3
anti-HA
250
130
ARF7
anti-GFP
Input
D
pCASP1::shy2-2 WT-SIM
Col-0
+SIM (L1)
+SIM (L2)
+SIM (L4)
pCASP1::shy2-2 non-SIM
Col-0
-SIM (L1)
-SIM (L2)
-SIM (L4)
E
IAA3
SUMO
Dry
ARF7
Wet
ARF7

Science
AAAS

Supplementary Materials for

Roots branch towards water by post-translational modification of transcription factor ARF7

Beatriz Orosa-Puente[1,7†], Nicola Leftley[2†], Daniel von Wangenheim[2†], Jason Banda[2], Anjil K Srivastava[1], Kristine Hill[2 +], Jekaterina Truskina[2,3], Rahul Bhosale[2], Emily Morris[2], Moumita Srivastava[1], Britta Kümpers[2], Tatsuaki Goh[2,4], Hidehiro Fukaki[4], Joop Vermeer[5], Teva Vernoux[3], Jose Dinneny[6], Andrew French[2], Anthony Bishopp[2], Ari Sadanandom[1*] & Malcolm Bennett[2*]

Correspondence to: Professor Ari Sadanonadom
Email: ari.sadanandom@durham.ac.uk; FON +44 191 33 41263

Professor Malcolm J. Bennett
Email: Malcolm.bennett@nottingham.ac.uk; FON +44 115 951 3255

This PDF file includes:

Materials and Methods
Supplementary Text
Figs. S1 to S22
Tables S1 to S3
Captions for Movies S1

Other Supplementary Materials for this manuscript include the following:

Movies S1

Materials and Methods

Plant material and growth conditions

Arabidopsis thaliana ecotype, Columbia (Col-0) was used as the wild-type control for all experiments except the *shy2-31* mutant (which is the Landsberg *erecta* background: L*er*-0). The *arf6-1* mutant and the GK798F08 set used to obtain *arf7-3* were provided by the Nottingham Arabidopsis Stock Centre, then the insertions confirmed by PCR using forward and reverse primers (obtained using T-DNA primer design tool) in combination with LBb1.3. The following mutant alleles: *arf7-1*, *arf8-2, arf19-1, ots1;2, lbd16-1, lbd16-2, shy2-31* and *pCASP1::shy2-2* Col-0 (previously published in (*18*) plus the reporter *pLBD16::LBD16-GFP* were used in LR hydropatterning bioassays and Light sheet imaging.

Arabidopsis thaliana seed lines were surface sterilized using 50 % (v/v) bleach for 7 min and two 0.001 % Triton X-100 washes followed five washes with sterile water and then stratified at 4 °C for 48 h in the dark. For LR hydropatterning bioassays, seeds were germinated on media containing ½ MS (2.2 g/L) (Murashige and Skoog media, Sigma), 0.5 g/L MES, 1 % sucrose and 1 % Bacto agar at pH 5.7. Seedlings were grown vertically for a minimum of 10 d (depending on the experimental design) under continuous temperature 22 °C with a 16 h photoperiod (150 µmol m^{-2} s^{-1}). The length of growth increased from 10 d to 13 d for the characterization of mutant alleles that displayed decreased LR numbers to ensure six LRs per seedling. Seedlings were scored based on their developmental growth prior to imaging the agar plates.

DNA constructs

All the constructs were generated by Gateway cloning technology. To generate the ARF7-GFP, IAA3/SHY2-HA, IAA14/SLR-HA, OTS1-HA, TIR1-GFP and TPL-Myc constructs, corresponding cDNA fragments were PCR amplified and cloned into pENTR/D-TOPO vectors (Supplemental Table. S1 and Table. S2). Recombination with Gateway recombinant cloning technology assembled the multiple DNA fragments to generate the various constructs used. The IAA3/SHY2 (SIM mutant) construct was generated with the aid of site-directed mutagenesis using gene specific primers.

Generating transgenic materials

pDONR^{201} ARF7 was cloned into a Gateway binary vector: *pGWB17* (*p35S 4xMyc*: previously published in (*21*) using Gateway cloning technology. The resulting plasmid was transformed into *Agrobacterium tumefaciens* GV3101 strain by electroporation and then transformed into *Arabidopsis thaliana arf7-1* plants by the floral dip method (*22*).

The *pARF7-mVenus-N7* was cloned using Gateway multisite cloning technology. The ARF7 fragment (−2973 to +374 bp) was PCR amplified using primers ARF7_For (aagagatgtcgcaaaccagc) and ARF7_Rev (cctttctcctgcattcacaca) and cloned into pCR8/GW/TOPO to create pARF7 pCR8/GW/TOPO. The later was recombined using a MultiSite Gateway reaction with the following plasmids: pDONR P4-P1R 5' MCS (an empty entry vector), pDONR P2R-P3 mVenusN7-35Sterm (containing mVenus coding sequences with the N7 nuclear

localization signal and a 35S CaMV terminator) and pK734GW (the destination vector contained the kanamycin resistance gene for *in planta* selection). The resulting plasmid was transformed into *Agrobacterium tumefaciens* C58pMP90 strain by electroporation and then transformed into *Arabidopsis thaliana* Col-0 plants by the floral dip method (*22*).

The translational reporter *pARF7::gARF7-mVenus* was cloned using both TOPO and MultiSite Gateway cloning technologies. The ARF7 fragment (−2973 to +4798 bp) incorporated the ARF7 promoter with gARF7 as a continuous fragment (7771 bp) minus the stop codon fused to G4S4-mVenus with an OcsT terminator pENTR P2RP3 (with a stop codon) and pK734GW (the destination vector contained the kanamycin resistance gene for *in planta* selection). The resulting plasmid was transformed into *Agrobacterium tumefaciens* GV3101 strain by electroporation and then transformed into *Arabidopsis thaliana* Col-0 and *arf7-1* plants by the floral dip method (*22*).

The *pARF7::ARF7-GFP* and *pARF7::ARF7^{4KR}-GFP* were both cloned using TOPO and MultiSite Gateway cloning technologies. The ARF7 promoter (-2973 to -1 bp) was fused with ARF7 cDNA and cloned into pENTR/D-TOPO. Site directed mutagenesis was used to mutate the SUMOylation sites within the *pARF7::ARF7* construct that was verified by sequencing. Both *pARF7::ARF7* and *pARF7::ARF7^{4KR}* were recombined into pGWB-GFP(C). The resulting plasmid was transformed into *Agrobacterium tumefaciens* by electroporation and then transformed into *Arabidopsis thaliana arf7-1* plants by the floral dip method (*22*). Expression of the ARF7-GFP protein was confirmed by western blot analysis with anti-GFP antibodies.

RNA Isolation and Quantitative RT-PCR

Total RNA was extracted from 10 d old seedlings grown in ½ MS media. Root tissue was then elicited with 1 μM NAA or water for 1 h and frozen in liquid nitrogen. A SpectrumTM Plant Total RNA kit (Sigma-Aldrich) was used to extract RNA following the manufacturer's recommendations. The RNA was then quantified by measuring the absorbance (260 and 280 nm) using a NanoDropTM 1000 Spectrophotometer (Thermo Scientific). The RNA was DNase treated (Promega DNase I) prior to cDNA synthesis, undertaken with Invitrogen SuperScript® II Reverse Transcriptase. The RNA was tested for the absence of contaminating genomic DNA by PCR, using primers spanning an exon junction. Quantitative PCR primers were designed for gene targets using the National Center for Biotechnology Information Primer-BLAST, and primer annealing temperatures tested using a gradient PCR. Relative expression was compared between genotypes, using target primers and primers for the housekeeping gene ACTIN7 (At5g09810) for normalization. Brilliant III Ultra-Fast SYBR QPCR MM (Agilent) was used in conjunction with Rotor- Gene® Q (Qiagen) and analysis was undertaken with the software provided using the comparative quantification method. At least four independent biological replicates were performed per experiment.

Agrobacterium mediated transient assays

Gene constructs were transiently expressed in *Nicotiana benthamiana* plants using the

Agrobacterium tumefaciens mediated transformation (*23*). ARF7-GFP and ARF7–GFP (4K/R) and GFP proteins were used to check the interactions with IAA3/SHY2-HA, IAA14/SLR-HA, OTS1-HA and TPL-myc in *Nicotiana benthamiana* leaves. 3 d post-infiltration, leaves were treated with either MgCl 10 mM or NAA for 30 min. Leaves were frozen in liquid nitrogen for sample preparation and co-immunoprecipitation performed.

Co-immunoprecipitation assay

Nicotiana Benthamiana plants were infiltrated with 10 mM MgCl2 or 5 μM NAA for 30 min. Total protein was then isolated for co-IP using the extraction buffer containing: 50 mM HEPES (pH7.5), 1 mM EDTA, 0.5% Trition-X 100 and 1 mM DTT. Anti-GFP IP and anti-myc IP were performed. Total protein was incubated with 50 μl anti-GFP beads (Chromotek) and put on ice for 30 min. The beads were then centrifuged at 10,000 g for 1 min and washed three times with 1 ml of cold IP buffer. After the last wash, 50 μl of pre-heated (95°C) 1× SDS-loading buffer was used to elute the immuno-complex. The immuno-complex was then analysed on a 10% SDS-PAGE gel using immunoblotting methods with Abcam (Cambridge, UK) anti-GFP, anti-HA antibodies (Anti-HA High Affinity, Sigma-Aldrich) and anti c-Myc (D84C12, Cell Signaling). At least three independent biological replicates were performed per experiment.

Immunoprecipitation assay

Arabidopsis thaliana seedlings (root tissue) were treated with 10mM MgCl2 or 1 μM NAA. Total protein from roots was isolated for IP using extraction buffer containing: 100 mM Tris-HCl (pH 8.0), 0.1% [w/v] SDS, 0.5% [w/v] Sodium deoxycholate, 1% [v/v] glycerol, 50 mM sodium metabisulfite, 20 mM N-Ethylmaleimide (NEM) and protease inhibitor cocktail. Anti-GFP IP was then performed. The total protein was mixed with 50 μl anti-GFP beads (Chromotek) and incubated on ice for 30 min. The beads were centrifuged at 10,000 g for 1 min and washed three times with 1 ml of cold IP buffer. After the final wash, 50 μl of pre-heated (95°C) 1× SDS-loading buffer was used to elute the immuno-complex that was then analyzed on a 10% SDS-PAGE gel using immunoblotting methods with anti-GFP (Abcam) (Cambridge, UK) and anti-SUMO1/2 antibodies, produced in the laboratory against AtSUMO1.

(Figure 2H):
Arabidopsis thaliana seedlings were grown for 4 weeks in Gamborgs B5 media, dried on paper towel and exposed to the air for 20 minutes at room temperature. Only the root tissue was used for immunoprecipitation (IP). Total protein from roots was isolated for IP using extraction buffer containing 100mM Tris-HCl, pH 8.0, 0.1% [w/v] SDS, 0.5% [w/v] Sodium deoxycholate, 1% [v/v] glycerol, 50 mM sodium metabisulfite, 20 mM N-Ethylmaleimide (NEM) and protease inhibitor cocktail (Roche). Anti-GFP IP was performed. Total protein extracts were incubated with 50 μl of anti-GFP beads (Chromotek anti-GFP beads) and incubated on ice for 30 min. The beads were then centrifuged at 10,000 g for 1 min and washed three times with 1 ml of ice-cold IP buffer. After the last wash 50 μl of pre-heated (95°C) 1× SDS-loading buffer was used to elute the immuno-complex. The immune-complex was then analysed on a 10% SDS-PAGE using immunoblotting methods with Abcam (Cambridge, UK) anti-GFP and anti-SUMO1/2 antibodies generated against AtSUMO1.

Chromatin immunoprecipitation

Chromatin immunoprecipitation was performed on root tissue of 10 d old seedling plants. 500 mg of tissue was crosslinked with 1% formaldehyde by vacuum infiltration for 7 min on ice. Cold glycine was added to a final concentration of 100 mM to quench crosslinking and a further vacuum infiltrated for 5 min. The crosslinked tissue was washed twice with ice cold water before all liquid removed and tissue frozen in liquid nitrogen. Nuclei were then isolated and lysed (previously described in (*12*) with the aid of sonication, performed using a BioRuptor Plus (Diagenode). Sonication consisted of 15 cycles of 30 s ON, 30 s OFF at high power. ARF7-GFP was immunoprecipitated using ChIP grade (Chromotek anti-GFP beads). Crosslink reversal and protein removal was performed (previously described in (*24*) by boiling, in the presence of Chelex 100 resin (BioRad), before incubation at 55°C with Proteinase K. Finally the DNA was cleaned up using PCR purification columns (Qiagen) and analyzed by qPCR using primers described in (*12*) (Supplemental Table S2). Data can be found in Supplemental Table. S3.

'Time course' ChIP

ChIP assays were performed using nuclei-enriched samples from root tissue pre-treated with 1 μM NAA for 0, 10 or 120 min and fixed under vacuum with 1% formaldehyde for 15 min. Nuclei were extracted and ChIP assays performed with anti-ARF19 or anti-ARF7 antibodies (previously described in (*25*). Briefly, 200 μl of sheared chromatin (average fragment size of 400 bp) was added to 1 ml Immunoprecipitation Buffer (50 mM Hepes, pH 7.5, 150 mM KCl, 5 mM MgCl2, 0.1% Triton X-100) and incubated along with 3 μg of anti-ARF19 or anti-ARF7 at 4°C. Protein G Dynabeads® (Invitrogen) were added and a further incubation at 4°C overnight. Input plus ARF7 or ARF19 immunoprecipitated DNA were used for qPCR with SYBR green master mix and primers (Supplemental Table S2). All qPCR reactions were performed as triplicate technical replicates using a Light Cycler 480 qPCR machine and are representative of three biological repeats.

Statistical Analysis

Statistical analysis of the data was performed using both a Student's *t*-test and ANOVA. The Student's *t*-test determined if the means of two data sets differed significantly from each other in relation to the null hypothesis. A different letter indicated a significant difference from that of WT (Col-0) roots based on the Student *t*-test *P* value ($P<0.05$).

ANOVA was used when there were more than two data sets to compare. The analysis of variance, one-way ANOVA took into account the total number of observations, means, standard deviations (or standard error) within each data set. Using GenStat, multiple comparisons, Tukey HSD (Honest Significant Difference) test was applied at the *P*-value 0.05 significance level (95% confidence interval) to each data set. Letters were used to indicate significance levels between all the data sets. Similar letters stated that there were no significant differences observed. Whereas, different letters indicated that there was a significant difference observed between the data sets ($P<0.05$).

Light Sheet Fluorescence Microscopy using the Zeiss Lightsheet Z.1

3D light sheet microscopy root outgrowth angle measurements (Figure 1B):
Arabidopsis thaliana seedlings were grown on the surface of media plates (½ MS + 1.2% phytagel + 0.97 g/L MES + 1% sucrose) for 7 d at 20–21 °C with a 16 h photoperiod (light intensity 150 µmol m^{-2} s^{-1}). Roots were carefully (without moving them) glued on the media plate using 1% agarose. 3 cm root segments from the root tip were cut out, including the media and transferred to a sample holder similar to the protocol previously described (*26*). Roots were imaged including the entire volume of the root as well as the gel substrate using a 405 nm laser. Auto-fluorescence was filtered using a 505-545 nm bandpass filter. Cross sections were used to measure the angle with which the primordium were growing out, in respect to the surface of the media. In order to distinguish between the contact and air sides, the auto-fluorescence of the media containing the gel was used.

Multi-view imaging (Figure 1C, D, S3):
Arabidopsis thaliana seedlings were grown on the surface of media plates (½ MS + 1.5% phytagel). Roots were covered with 1% agarose containing fluorescent beads (PS-Speck, fluorescent beads, ThermoFisher, Catalog number: P7220) and further processed according to the protocol depicted in Supplemental Fig. S5a. Roots were imaged with a Zeiss Lightsheet Z1 microscope. Images were captured using the W Plan-Apochromat 20x/1.0 and the PCO.edge camera module (CMOS, 1920x1920 pixel). Excitation wavelengths: 488 nm for GFP and 514 nm for YFP. Emission filter: Bandpass 505-545 nm for GFP and Bandpass 525-545 nm for YFP. Multi-view images were set up using the Quick-Setup option in the ZEN software. Single views were fused using the bead-based registration using the Fiji plugin Multiview Reconstruction (*27*, *28*). Final voxel size of fused image data sets is 0.43 μm^3. Details of the data analysis is described in Figure S5 and S6.

Confocal microscopy using the Leica SP5

Arabidopsis thaliana seedlings were grown on the surface of media plates (½ MS + 1.0% bactoagar + 0.5 g/L MES + 1% sucrose) for 7 d at 20–21 °C with a 16 h photoperiod (light intensity 150 µmol m^{-2} s^{-1}). Seedlings were carefully transferred to a microscope slide and stained with a propidium iodide solution (15 µg ml^{-1}) to visualize the cell walls before the addition of a cover slip. Confocal microscopy was performed using a Leica SP5 confocal laser scanning microscope (Leica Microsystems). Roots were imaged from the root tip to the shoot using the argon 488 nm laser (YFP/PI). Images were viewed, maximum projection applied (if necessary), snapshot(s) taken and final image(s) exported as a JPEG using the Leica application suite (LAS) AF Lite software.

LR hydropatterning phenotyping bioassay

In order to quantify the direction of lateral root emergence in respect to the surface of an agar plate, a LR hydropatterning phenotyping bioassay was devised by (*4*). LRs were visualized using a dissecting microscope and characterized into two different phenotypic groups: contact or air side. The group that the LR was assigned to was based on its initial direction of emergence from the

PR, when observing the *Arabidopsis thaliana* seedling from above. LRs were characterized as emerging from the contact side if the point of emergence could not be seen from above and was below the root horizon. These LRs also appeared to be out of focus near the PR. LRs within the air side group were characterized as growing upwards towards the microscope. There were also LRs that would emerge just above the horizontal axis. These LRs were considered to be within the air category if the meniscus (seen when LRs grow across the agar plate) was not present and there was a greater degree of angle upwards. In relation, there also had to be rings seen underneath the emerged LR, almost like a tree branch, with a degree of angle upwards. This ensured that emerged LRs on the horizontal axis (considered as contact), that displayed no meniscus, were not characterized incorrectly.

Lateral root density

Images of whole plates were taken using a Canon digital camera. PR length was measured using the NeuronJ plugin in ImageJ. LR number was counted manually and LR density was calculated by dividing LR number by the length of the root.

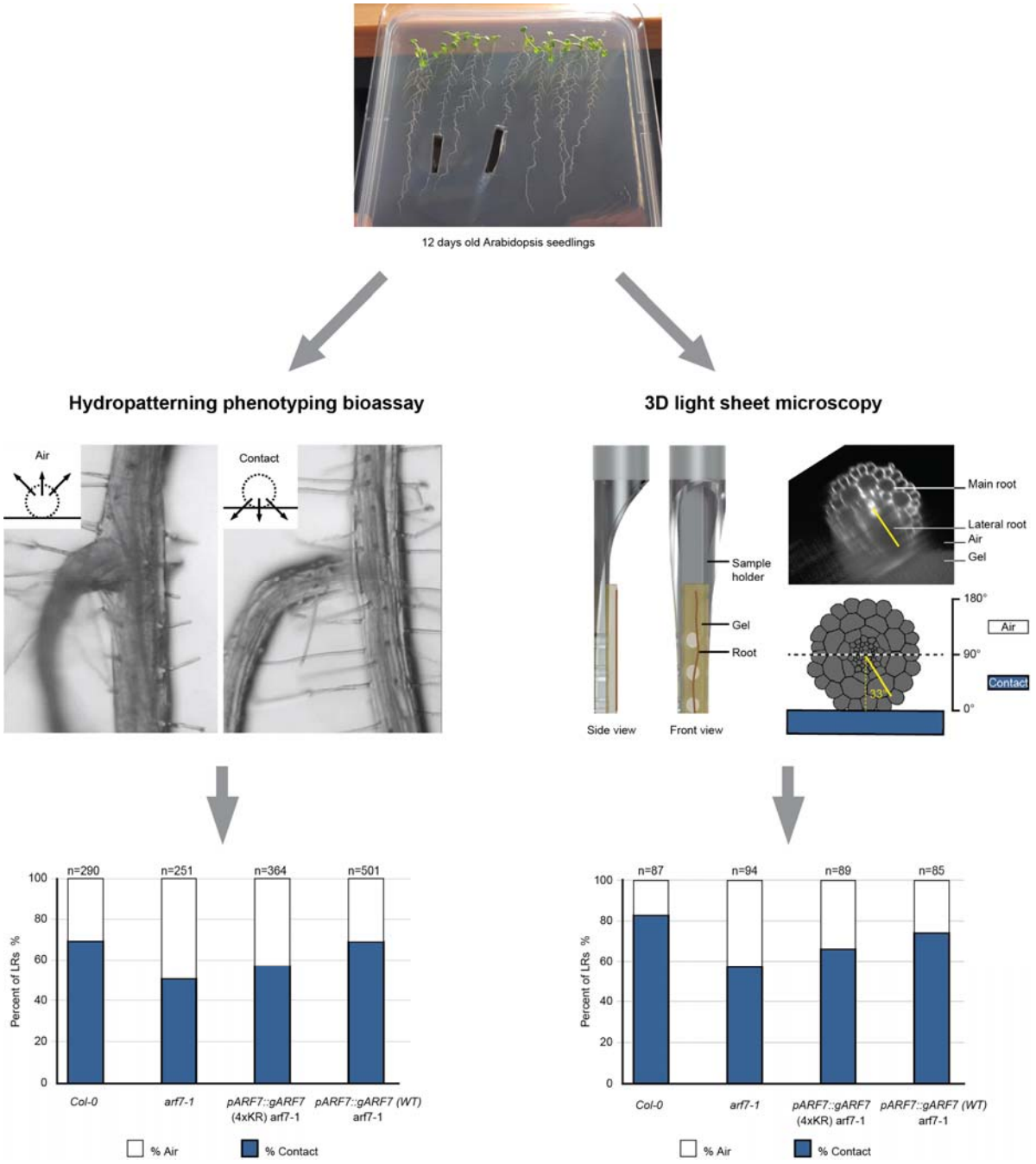

Fig. S1. Quantification of lateral root outgrowth site with respect to the surface of agar.
Hydropatterning experiments were routinely performed along the length of the mature root after LRs had emerged using the "Hydropatterning phenotyping bioassay". To validate this bioassay, we performed "3D light sheet microscopy root outgrowth angle measurements". We compared the results performed with both methods on the very same plants and found comparable results. The methods are described in more detail in the material and methods section.

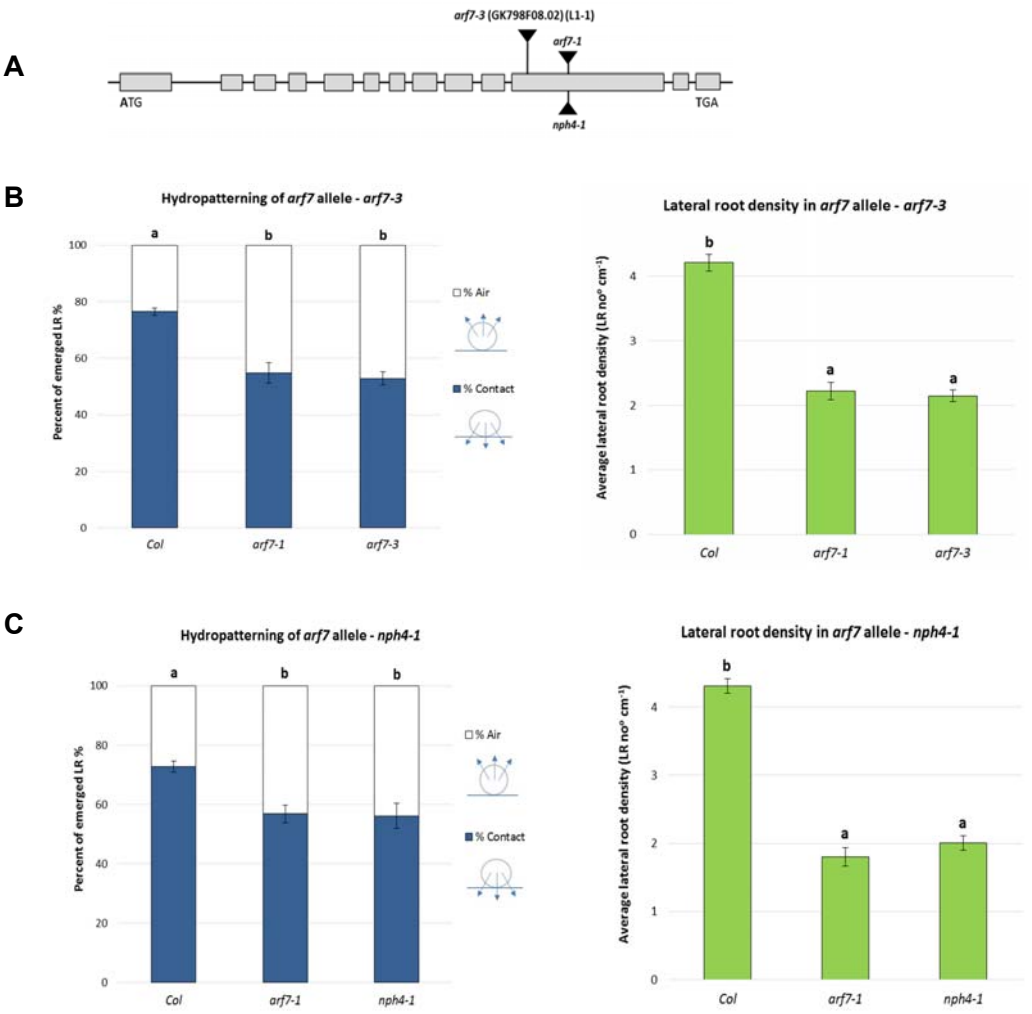

Fig. S2. Multiple independent *arf7* loss of function alleles exhibit a hydropatterning defect.
(**A**) Schematic representation of the *ARF7* (At5g20730) gene structure (5644 bp) and the positioning of *arf7* mutations: *arf7-1* (Salk T-DNA) (11th Exon), *arf7-3* (GK798F08.02) and *nph4-1* (11th Exon). Exons (boxes) and introns (lines) were determined by comparing the full length DNA sequence with that of nucleotide sequences of *arf7* mutant alleles. (**B**) & (**C**) The *arf7-1*, *arf7-3* (GK798F08.02) and *nph4-1* mutants exhibit LR hydropatterning and density defects. Data shown is mean values ± S. E. Statistical differences were analyzed on the percent of emerged LRs emerging towards either contact or air using an Anova, Tukey HSD test (P<0.05); statistically similar groups are indicated using the same letter. The 2 independent experiments shown above feature WT >70% contact and *arf7-1* <60%, as the positive and negative controls. (B) n LR=355/208/221 n Plants=9/11/13, (C) n LR=341/171/244 n Plants=10/11/13.

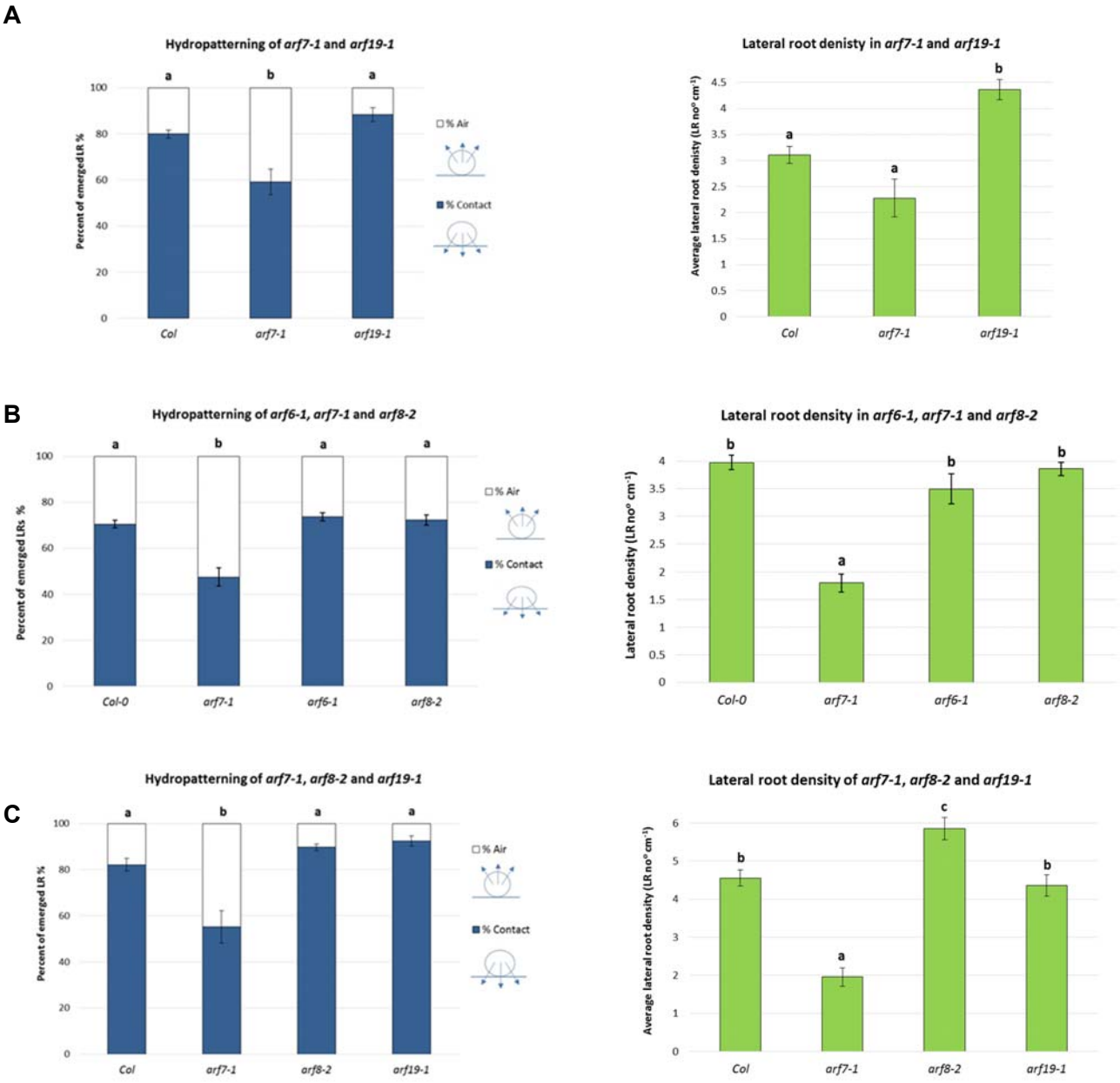

Fig. S3. Mutants lacking ARF6, ARF8 or ARF19 do not exhibit a hydropatterning defect.

The *arf7-1* mutant exhibited a hydropatterning defect that was not observed in *arf6-1*, *arf8-2* and *arf19-1 lof* mutant alleles. Data shown is mean values ± S. E. Statistical differences were analyzed on the percent of emerged LRs emerging towards either contact or air using an Anova, Tukey HSD test (P<0.05); statistically similar groups are indicated using the same letter. The 3 independent experiments shown above feature WT >70% contact and *arf7-1* <60%, as the positive and negative controls. (A) n LR=147/127/191 n Plants=9/11/8, (B) n LR=374/175/179/308 n Plants=11/11/7/9, (C) n LR=165/81/186/178 n Plants=7/8/6/7.

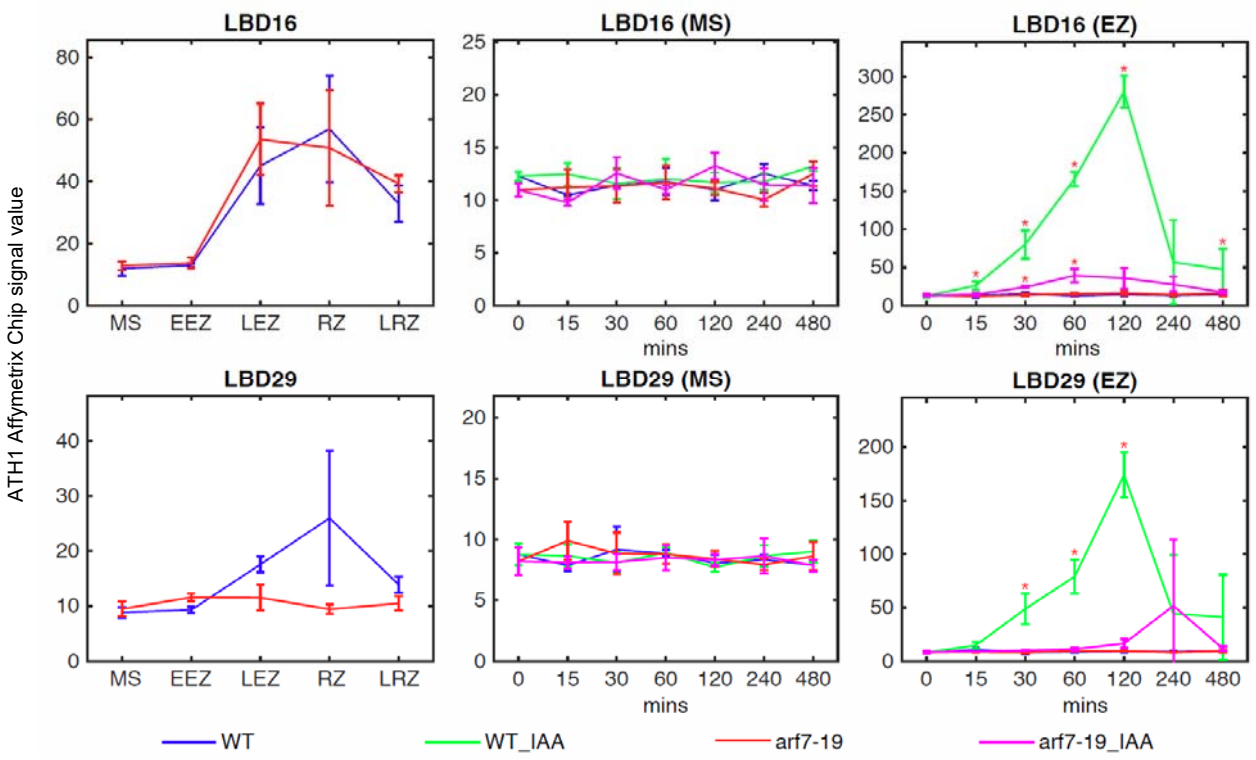

Fig. S4. *LBD16* & *LBD29* auxin inducible expression is ARF7 & ARF19 dependent.

Primary root zones of WT and *arf7-1 arf19-1* mutant lines were micro-dissected following 0 and 1 µM IAA treatments after 0, 15, 30, 60, 120, 240 and 480 min. Line graphs represent transcript abundances of *LBD16* and *LBD29* profiled using ATH1 Affymetrix Chip. The x-axis (left panels) denotes root zone samples which include MS: Meristem, EEZ: early elongation zone, LEZ: late elongation zone, RZ: root hair zone, LRZ: lateral root zone. * Indicates significant difference (P-value < 0.05) judged by Student's *t*-test and after Benjamini and Hochberg False discovery rate correction.

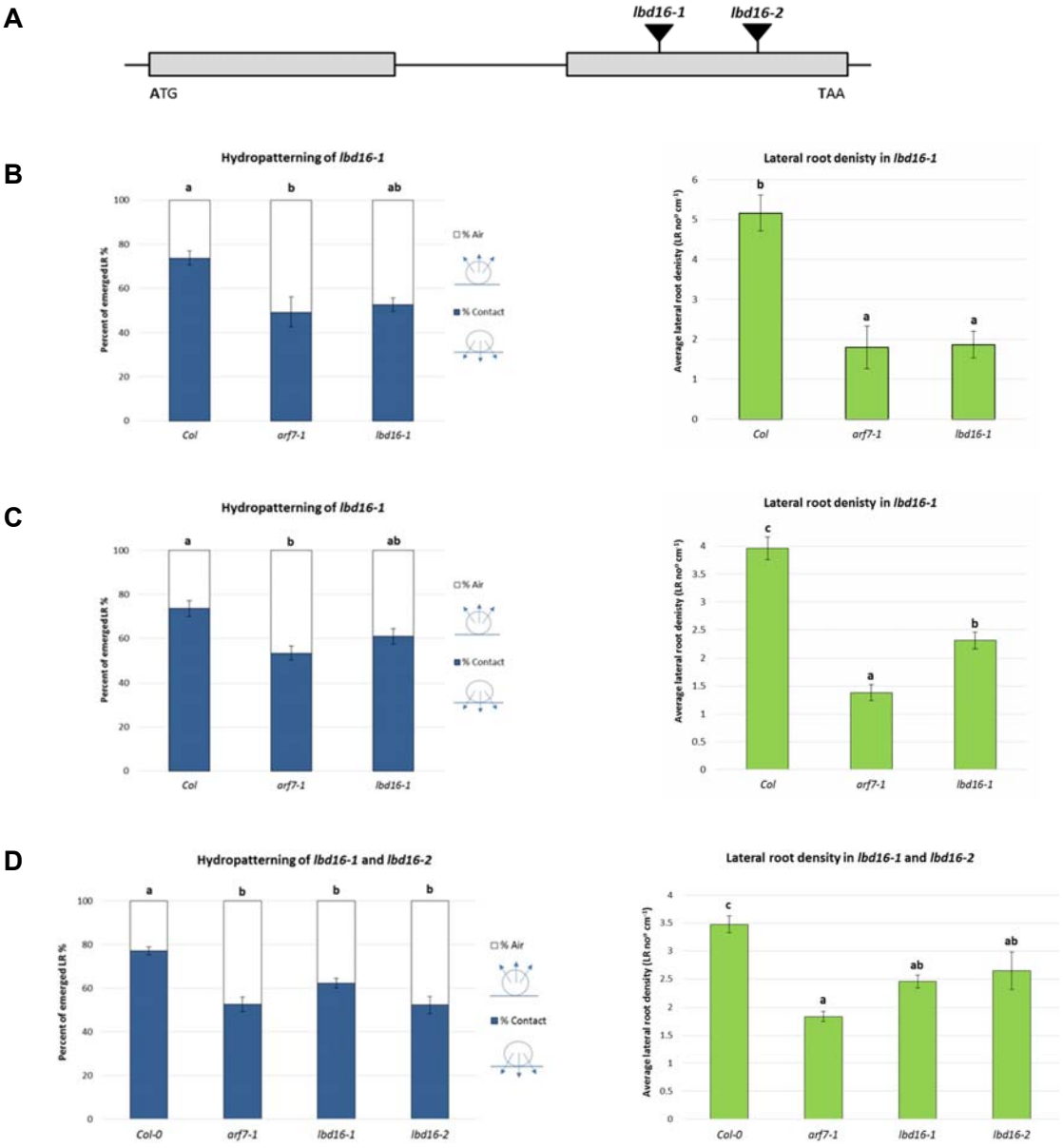

Fig. S5. LBD16 is required for hydropatterning.

(**A**) Schematic representation of the *LBD16* domain structure specifying *lbd16* alleles. *LBD16* gene (At2g42430) (1985 bp) and the positioning of *lbd16* mutations: *lbd16-1* (Salk_095791) (2nd Exon) and *lbd16-2* (Salk_040739) (2nd Exon). The location of the start (ATG) and stop (TAA) codons have been indicated. Exons (boxes) and introns (lines) were determined by comparing the full length DNA sequence with that of nucleotide sequences of *lbd16* mutant alleles (https://www.arabidopsis.org). (**B**) WT (Col-0) *Arabidopsis thaliana* roots exhibit a LR hydropatterning response that was disrupted by both *lbd16-1* and *lbd16-2 lof* mutant alleles and density defects. Data shown is mean values ± S. E. Statistical differences were analyzed on the percent of emerged LRs emerging towards either contact or air using an Anova, Tukey HSD test ($P<0.05$); statistically similar groups are indicated using the same letter. The 3 independent experiments shown above feature WT >70% contact and *arf7-1* <60%, as the positive and negative controls. (A) n LR=183/92/39 n Plants=7/9/4, (B) n LR=188/137/240 n Plants=9/17/22, (C) n LR=290/168/212/158 n Plants=9/9/10/7.

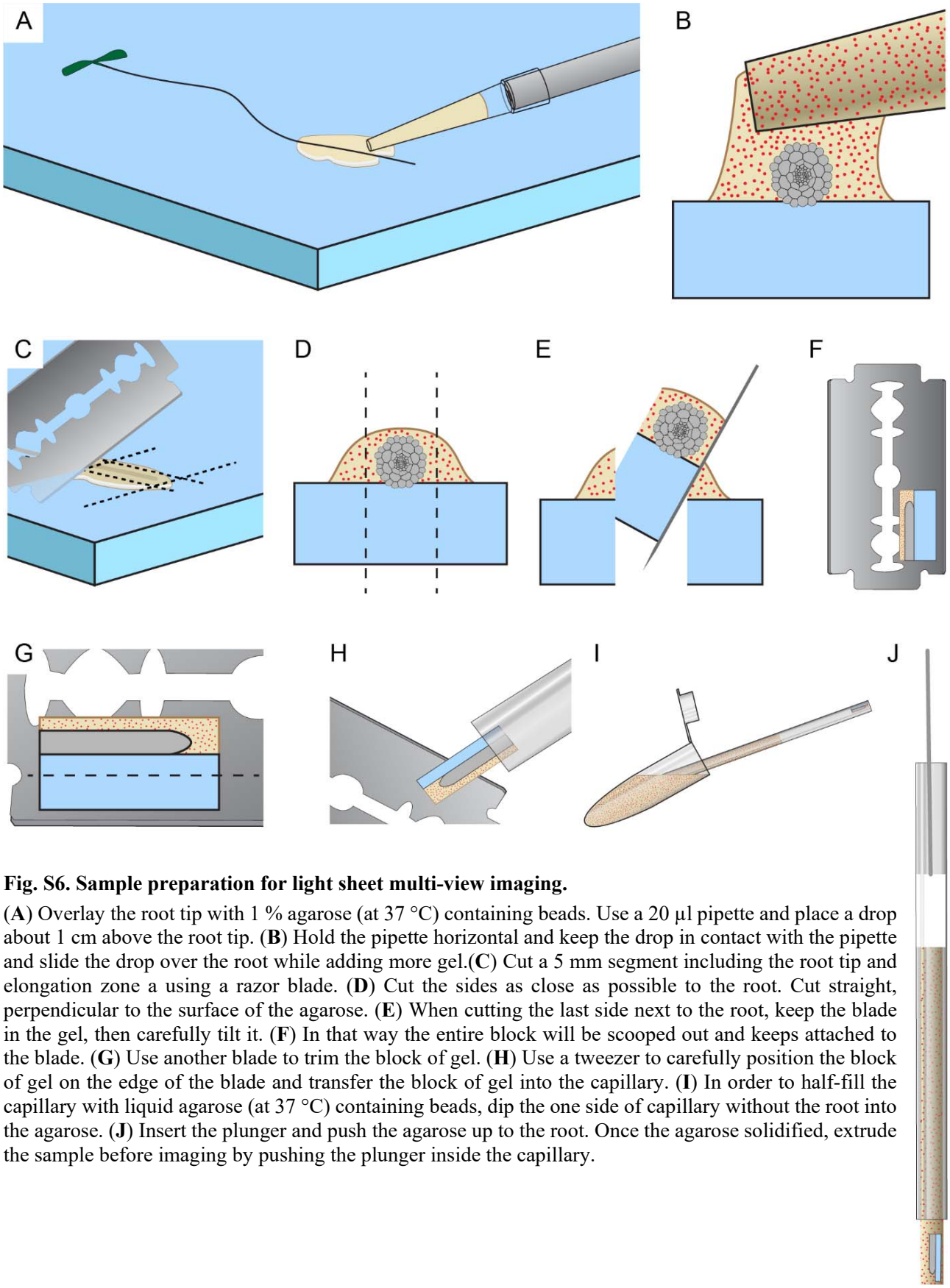

Fig. S6. Sample preparation for light sheet multi-view imaging.

(**A**) Overlay the root tip with 1 % agarose (at 37 °C) containing beads. Use a 20 µl pipette and place a drop about 1 cm above the root tip. (**B**) Hold the pipette horizontal and keep the drop in contact with the pipette and slide the drop over the root while adding more gel.(**C**) Cut a 5 mm segment including the root tip and elongation zone a using a razor blade. (**D**) Cut the sides as close as possible to the root. Cut straight, perpendicular to the surface of the agarose. (**E**) When cutting the last side next to the root, keep the blade in the gel, then carefully tilt it. (**F**) In that way the entire block will be scooped out and keeps attached to the blade. (**G**) Use another blade to trim the block of gel. (**H**) Use a tweezer to carefully position the block of gel on the edge of the blade and transfer the block of gel into the capillary. (**I**) In order to half-fill the capillary with liquid agarose (at 37 °C) containing beads, dip the one side of capillary without the root into the agarose. (**J**) Insert the plunger and push the agarose up to the root. Once the agarose solidified, extrude the sample before imaging by pushing the plunger inside the capillary.

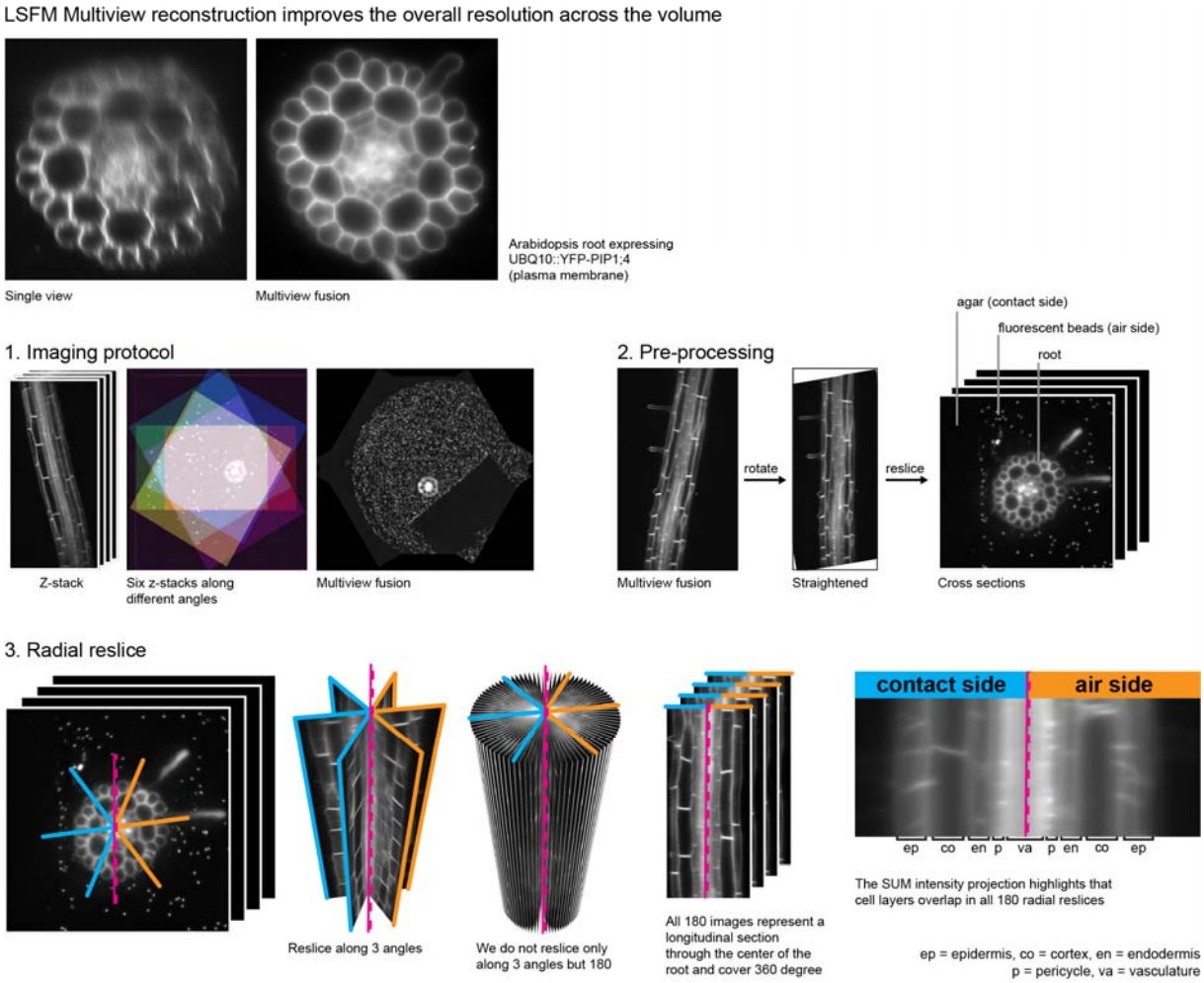

Fig. S7. Image analysis methodology for hydropatterning using the LSFM.

Multiview acquisition was used to capture 3D image z-stacks along six angles using the Zeiss Lightsheet Z1. *Arabidopsis thaliana* roots were mounted as shown in Fig. S6. (**1**) Acquired Zeiss CZI-files were fused using the Fiji plugin Multi-view Reconstruction (*27*, *28*). (**2**) In order to straighten the root in 3D, the fused stacks were rotated using the "Interactive Stack Rotation" tool in Fiji. Cross section were obtained through the "Reslice" function in Fiji. (**3**) The radial reslice was then used to generate 180 longitudinal sections displaced at 1 degree across the radius of the root. In that way the left side of all 180 reslices derives from one half of the root and the right hand side contains the other half. In the resulting stack of images concentric tissue cell layers overlap.

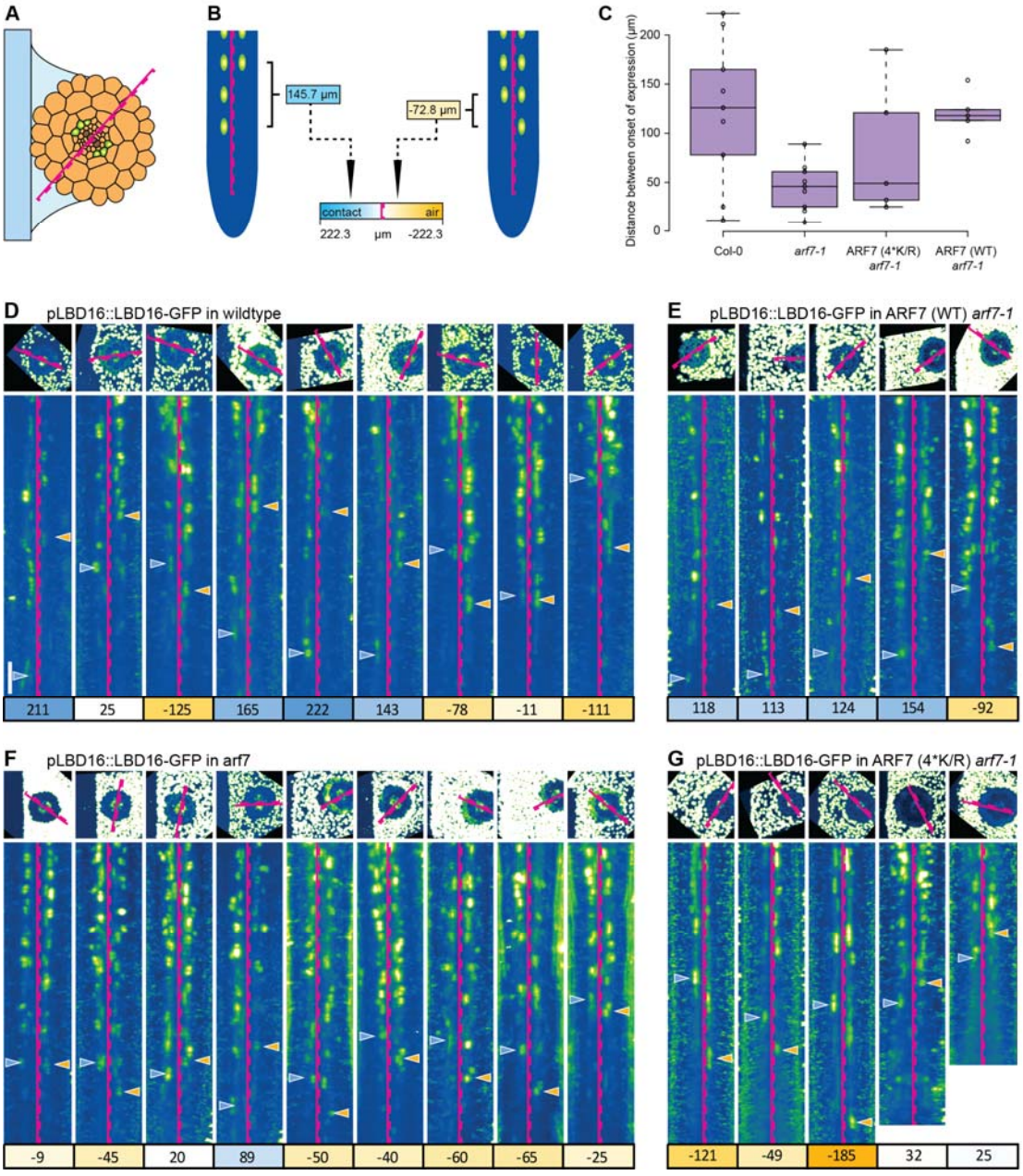

Fig. S8. LBD16-GFP is expressed asymmetrically in wildtype but not *arf7-1* background.

Images were generated and processed according to the description in Fig. S6 and S7. Individual images show the onset of LBD16 expression in the elongation zone of an Arabidopsis root. (**A**) In order to capture and quantify the *LBD16-GFP* expression above each of both xylem poles separately, a line (pink) was drawn in between the two xylem poles. The xylem pole facing the contact side is on the solid side of the pink line; the other xylem pole in contact with air is on the dashed side of the pink line. (**B**) The distance between the onsets of expression (first visible nucleus from the tip) on both sides was measured and displayed under each image. (C) Quantification of the data shown in D, E, F an G (**D-G**) The upper panels represents a cross section (SUM projection of 400 slices). Lower panels show a maximum intensity projection of the 180 radial reslices.

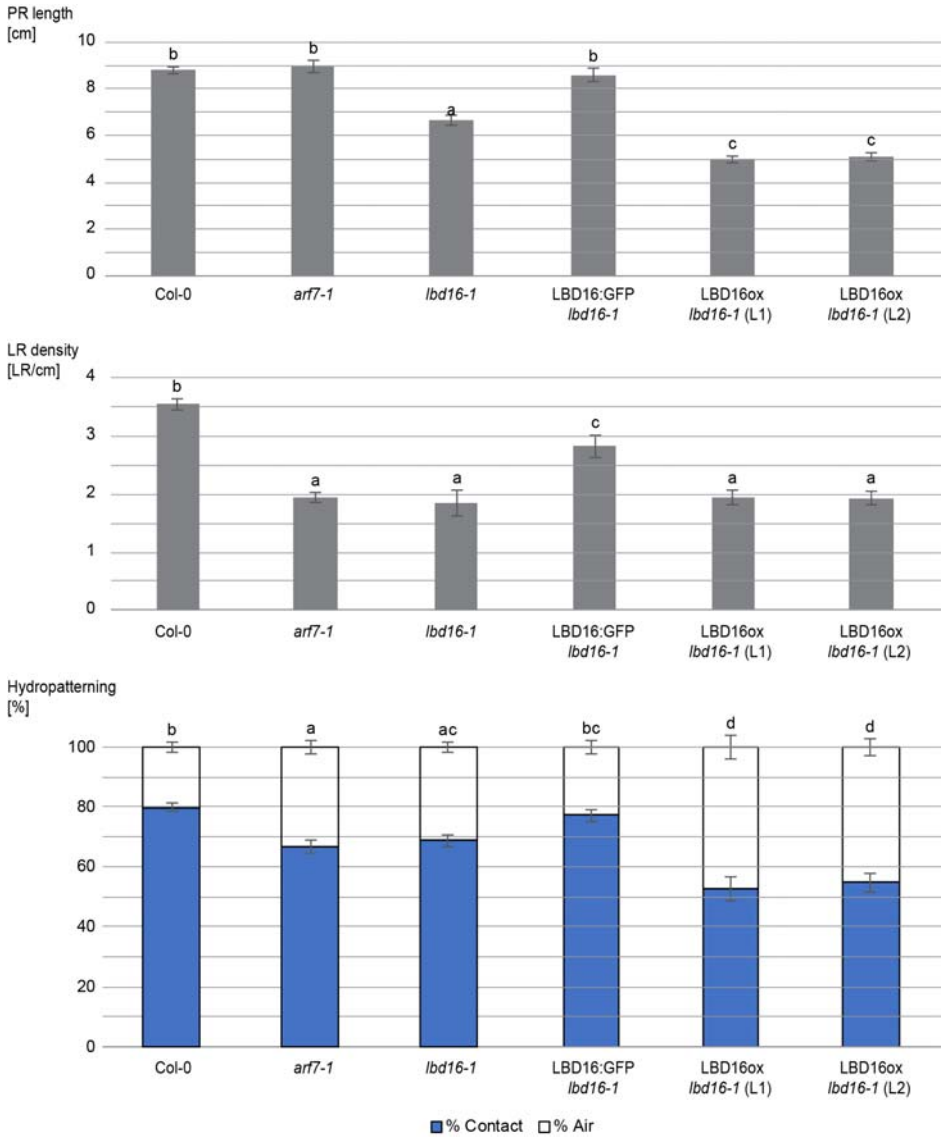

Fig. S9. LBD16 overexpression lines does not rescue the *lbd16* hydropatterning defect
Both *p35S:LBD16 lbd16-1* transgenic lines exhibited a hydropatterning and density defects that are not observed in *pLBD16::LBD16-GFP lbd16-1* or WT (Col-0) roots. Data shown is mean values ± S. E. Statistical differences were analyzed on the percent of emerged LRs emerging towards either contact or air using an Anova, Tukey HSD test ($P<0.05$); statistically similar groups are indicated using the same letter, n LR=498/313/155/382/126/129 n Plants=17/18/12/15/13/13

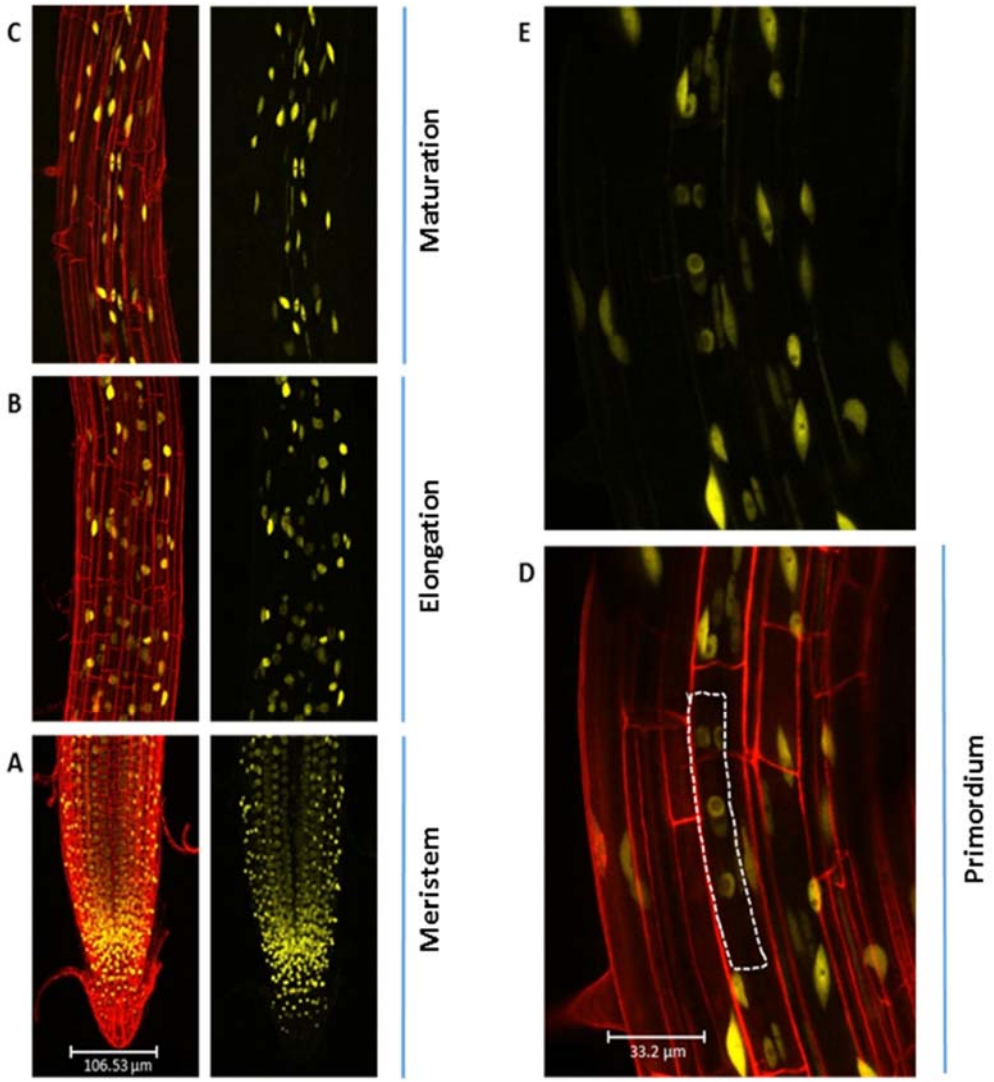

Fig. S10. Spatial expression patterns of the *pARF7::mVenus* reporter.

Root spatial expression patterns of a *pARF7::mVenus* reporter line. The *ARF7* transcriptional reporter exhibited bright Venus expression in nuclei throughout *Arabidopsis thaliana* root tissues. Reporter expression was detected in every tissue of the root apical meristem (**A**), elongation zone (**B**) and the maturation zone (**C**). Venus reporter expression was present in pericycle cells (denoted by white dotted line in **D**) from which LRP originate (**D**, **E**). Images are maximum projections of confocal image stacks. Scale bars – approx. 100 µm (**A** to **C**) and approx. 30 µm (**D** and **E**).

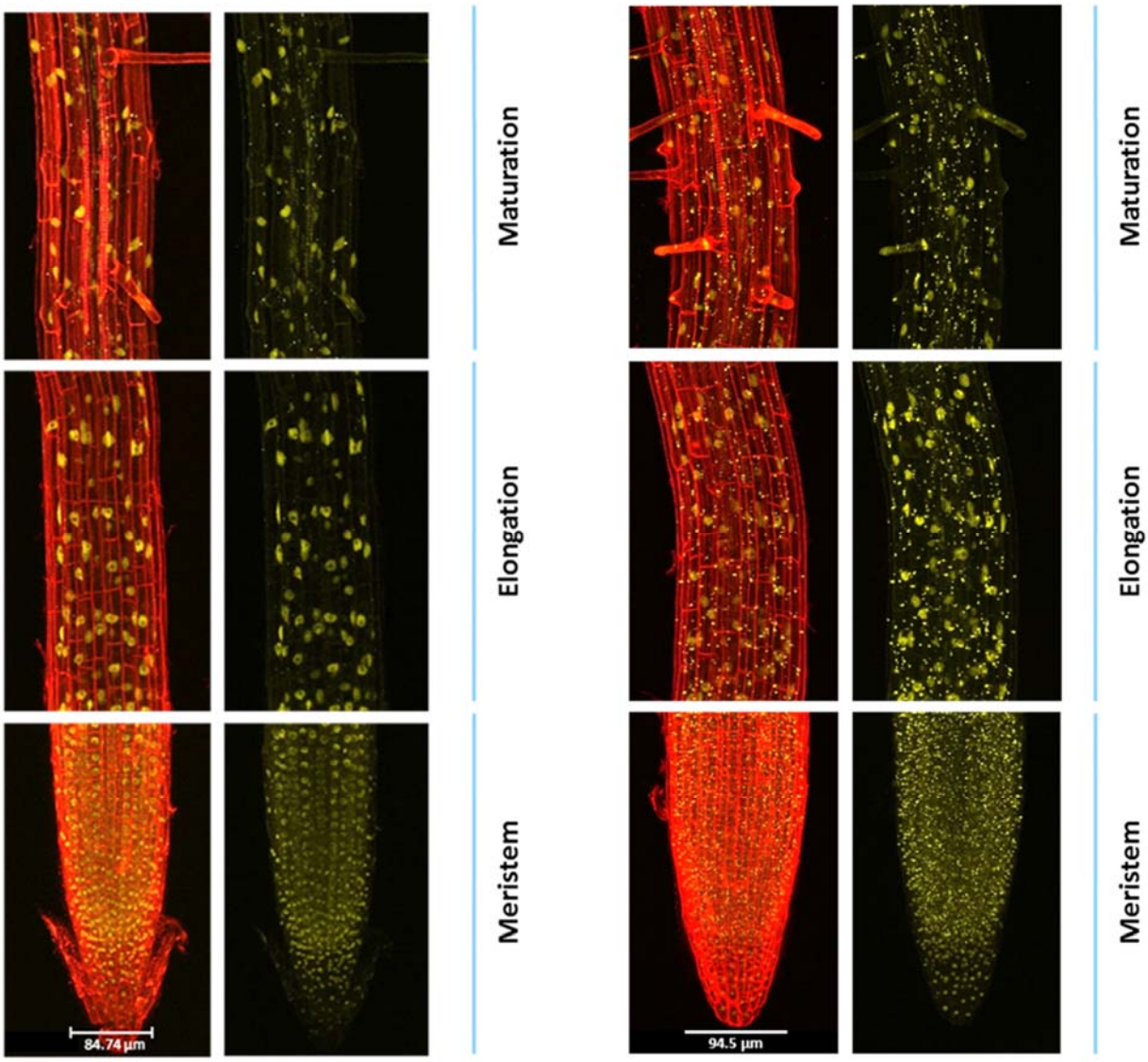

Fig. S11. Spatial expression patterns of *gARF7-mVenus* reporter lines.
gARF7-mVenus translational reporter lines exhibited Venus signal in cells throughout *Arabidopsis thaliana* roots. Expression was detected in all tissues of the RAM, elongation zone and maturation zone. A total of 7 *gARF7-mVenus* lines were isolated. 4 lines showed no Venus signal, perhaps due to silencing of the construct. The remaining 3 lines exhibited a pattern consistent with the expression of the transcriptional construct in Fig. S7. 2 of these lines showed a predominantly speckled pattern with the protein accumulating in an unknown cellular compartment (see right hand side panels). One line showed a predominantly nuclear expression pattern (left hand panel). Similar results were obtained when Venus was attached to the N terminus. Images are maximum projections of confocal image stacks. Scale bar, approx. 85-95 µm.

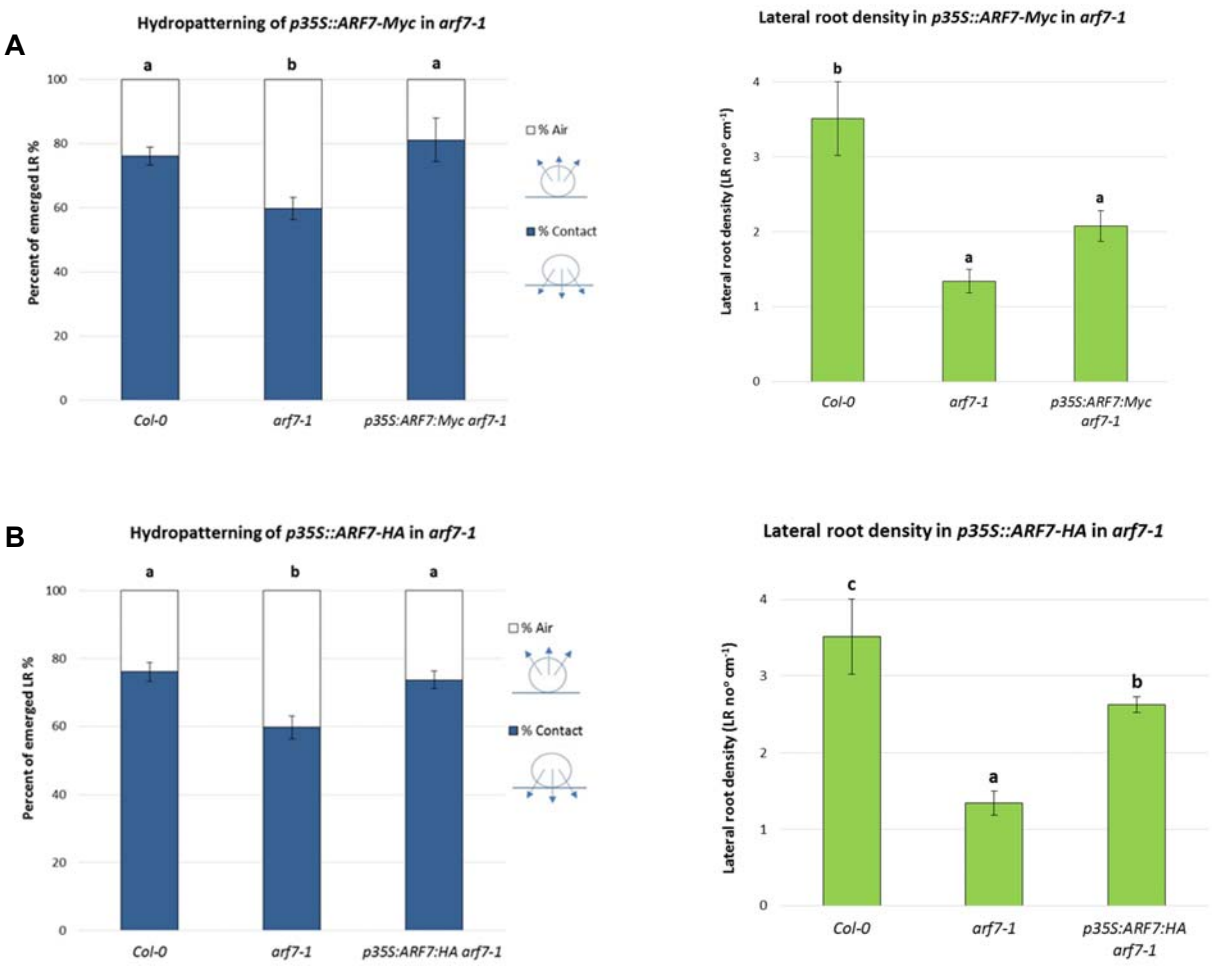

Fig. S12. Over-expression of ARF7 in *arf7-1* was able to rescue *arf7-1* LR hydropatterning defect. The percent of LRs emerging towards the air and contact sides in the *p35S::ARF7-Myc arf7-1* (A) and *p35S::ARF7-HA arf7-1* (B) transgenic lines were similar to WT (Col-0) roots. Data shown is mean values ± S. E. Statistical differences were analyzed on the percent of emerged LRs emerging towards either contact or air using an Anova, Tukey HSD test ($P<0.05$); statistically similar groups are indicated using the same letter. The 2 independent experiments shown above feature WT >70% and *arf7-1* <60% contact, as the positive and negative controls. (A) n LR=121/121/73 n Plants=4/10/4, (B) n LR=121/121/326 n Plants=4/10/14.

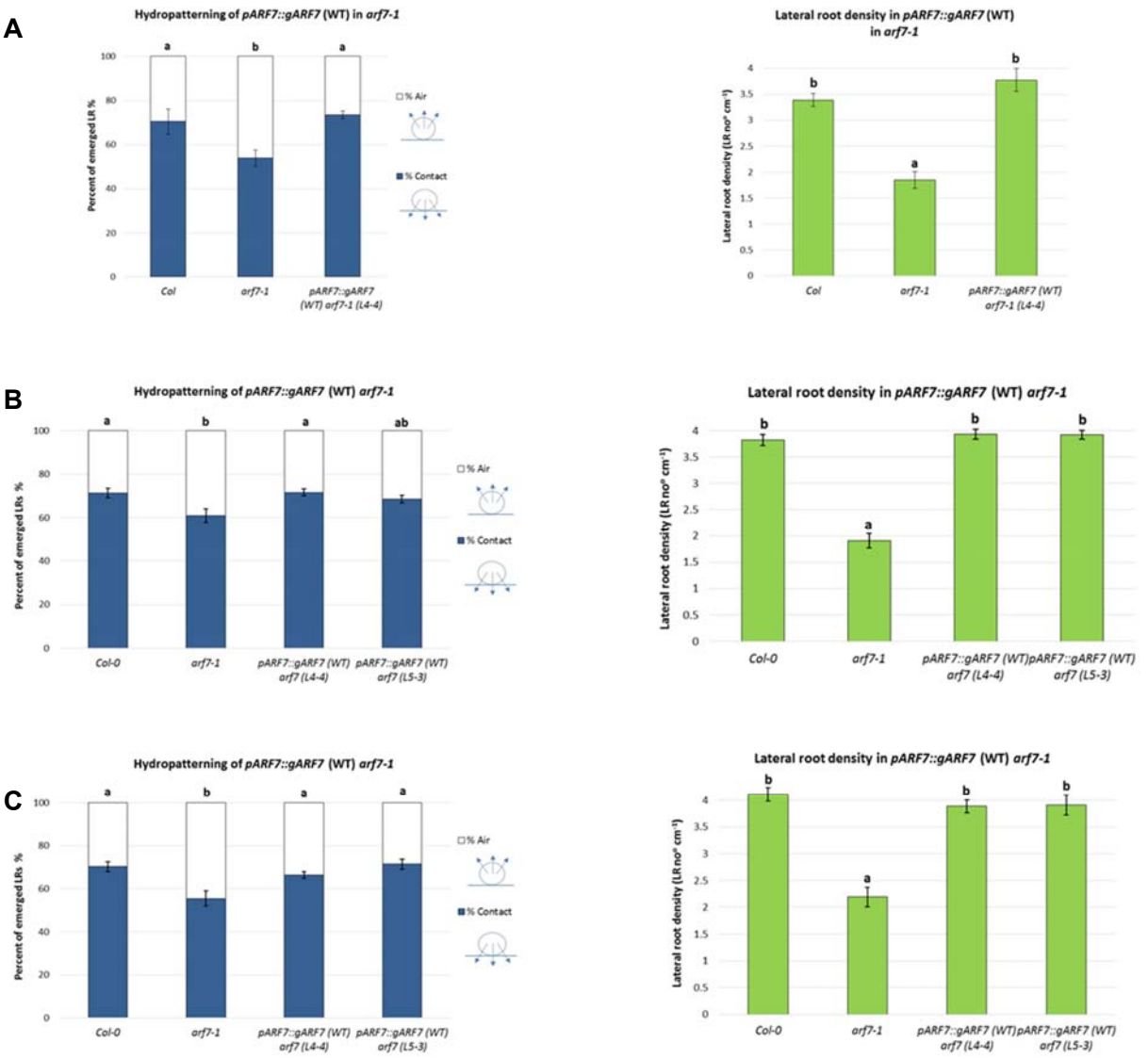

Fig. S13. The *arf7-1* hydropatterning defect was rescued by *gARF7*

Two independent transgenic lines expressing *gARF7* (termed L4-4 and L5-3) were able to rescue the *arf7-1* hydropatterning defect (left) and the *arf7-1* LR density defect (right) back to a WT level. Data shown is mean values ± S. E. Statistical differences were analyzed for both the percent of emerged LRs emerging towards either contact or air and LR density using an Anova, Tukey HSD test ($P<0.05$); statistically similar groups are indicated using the same letter. The 3 independent experiments shown above feature WT >70% and *arf7-1* <60% contact, as the positive and negative controls. (A) n LR=241/144/347n Plants=8/8/11, (B) n LR=462/235/661/607 n Plants=13/13/18/17, (C) n LR=498/207/505/178 n Plants=15/11/16/6.

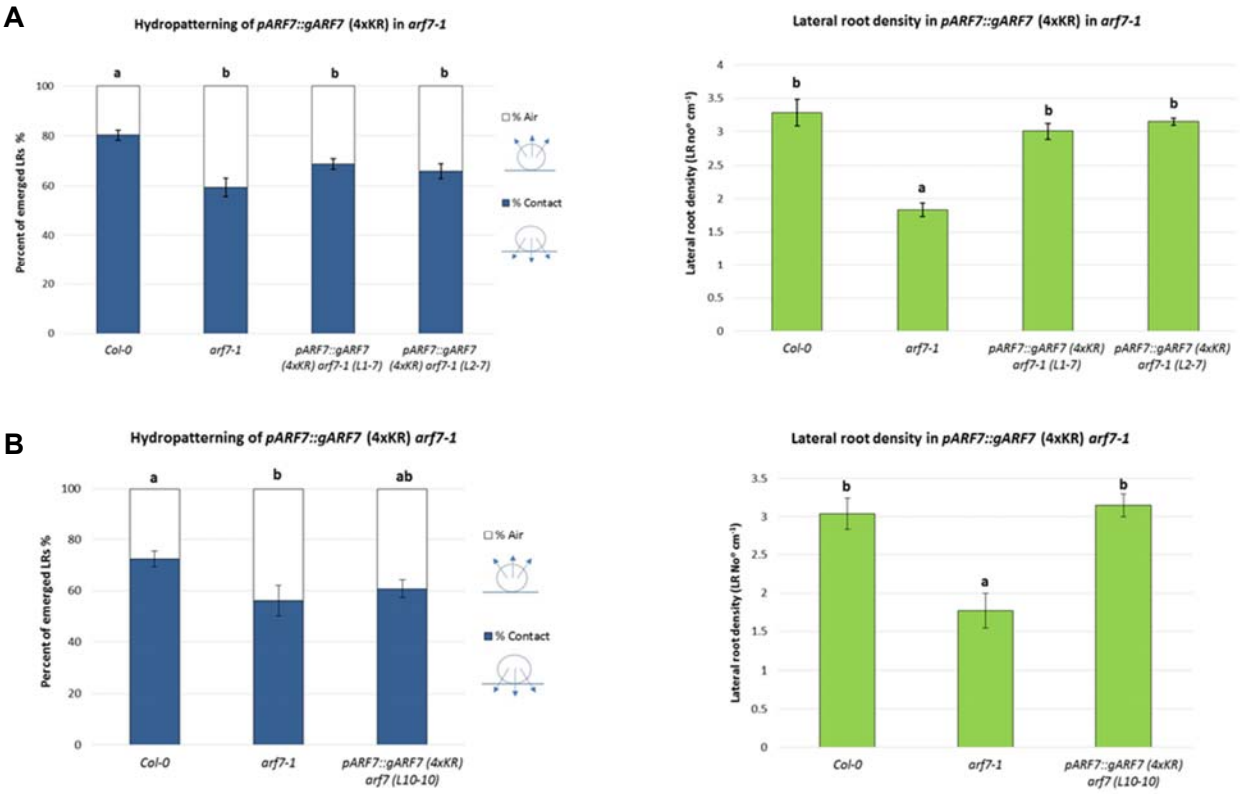

Fig. S14. The *arf7-1* hydropatterning defect was not rescued by *gARF7*$^{4K/R}$
Three independent transgenic lines expressing *gARF7*$^{4K/R}$ (termed L1-7, L2-7 and L10-10) were not able to rescue the *arf7-1* hydropatterning defect (left); but did restore the *arf7-1* LR density defect back to a WT level (right). Data shown is mean values ± S. E. Statistical differences were analyzed for both the percent of emerged LRs emerging towards either contact or air and LR density using an Anova, Tukey HSD test (P<0.05); statistically similar groups are indicated using the same letter. The 2 independent experiments shown above feature WT showing >70% contact and *arf7-1* <60%, as positive and negative controls. (A) n LR=434/307/296/285 n Plants=15/17/12/10, (B) n LR=196/78/250 n Plants=7/5/9.

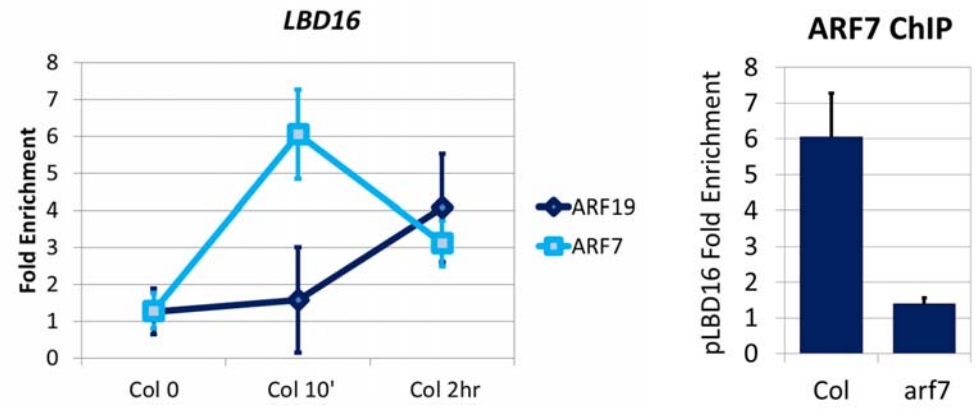

Fig. S15. LBD16 is a direct target of ARF7
Time course ChIP-PCR analysis revealed ARF7 transiently interacts with the *LBD16* target promoter following auxin treatment. Fold enrichment was calculated as the amount of *LBD16* promoter fragments immunoprecipitated, relative to the non-immunoprecipitated input chromatin. The same nuclear preps were used for both ARF7 and ARF19 ChIP assays. Unlike ARF19, ARF7 expression is stable following auxin treatment both at the mRNA and protein levels. The enhanced binding with ARF19 is unsurprising, given increased protein levels following NAA treatment.

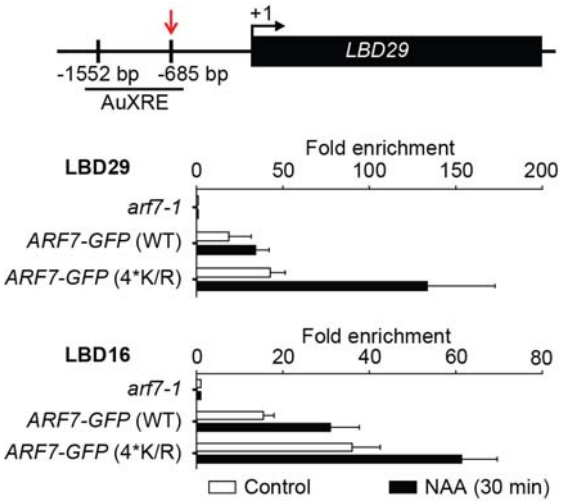

Fig. S16. ChIP-PCR assays

ChIP-PCR analysis was performed on roots of *arf7-1*, *arf7-1* ARF7-GFP or arf7-1ARF7-GFP (4*K/R) treated with 1 μM NAA for 30 min. DNA binding to AuxRE motifs in LBD29 (-685) and LBD16 (-989) promoters was expressed as fold enrichment. Data points represent mean ± SD (n=4).

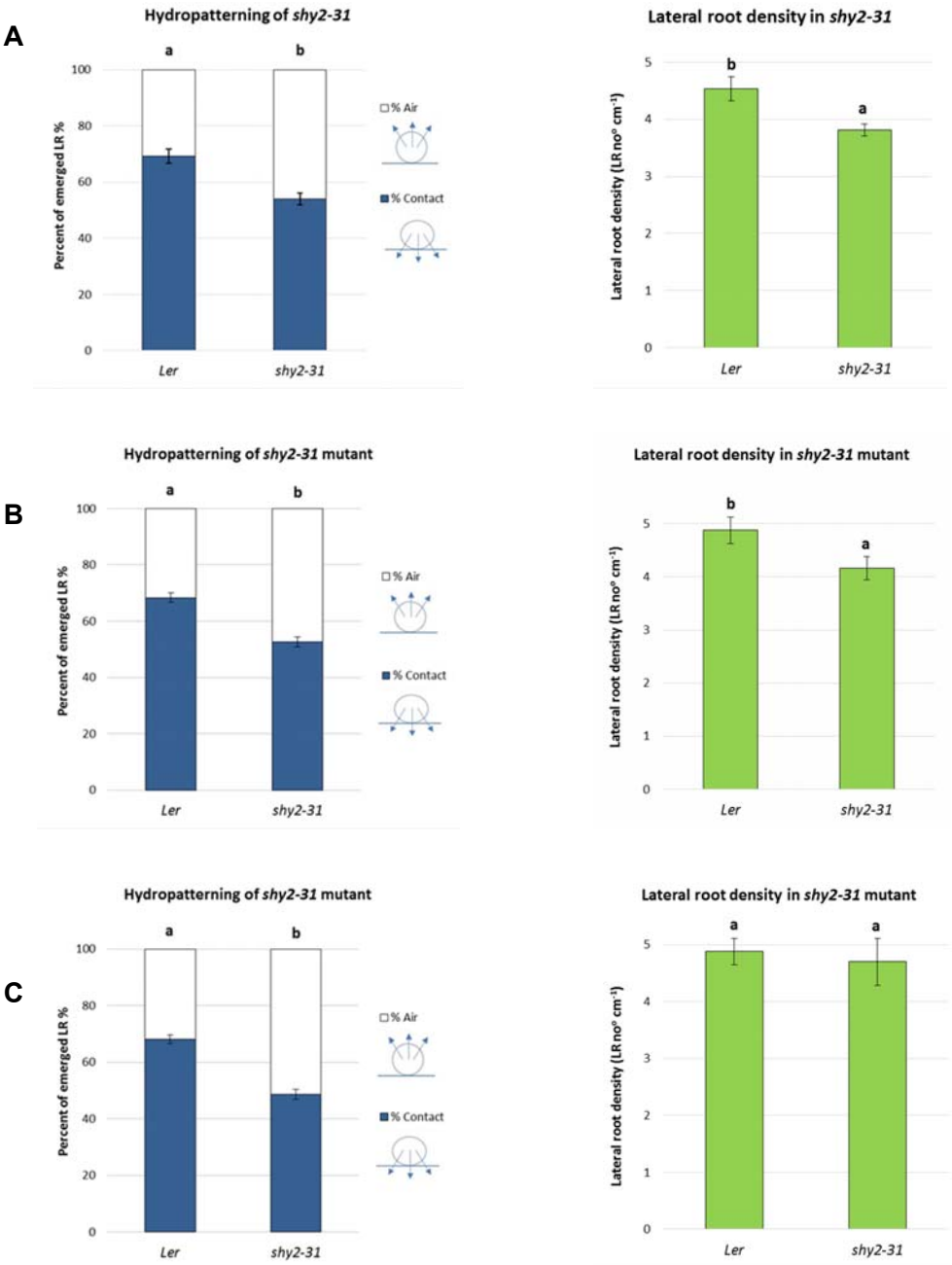

Fig. S17. *IAA3/SHY2* is required for LR hydropatterning.

The *Arabidopsis thaliana* WT (L*er*) hydropatterning response was disrupted in the *shy2-31* mutant allele. Data shown is mean values ± S. E from 3 different experiments. Letters indicate a significant difference compared to that of WT (L*er*) roots based on using a Student's *t*-test ($p<0.05$). (A) n LR=315/215 n Plants=10/7, (B) n LR=514/443 n Plants=18/15, (C) n LR=584/405 n Plants=14/10.

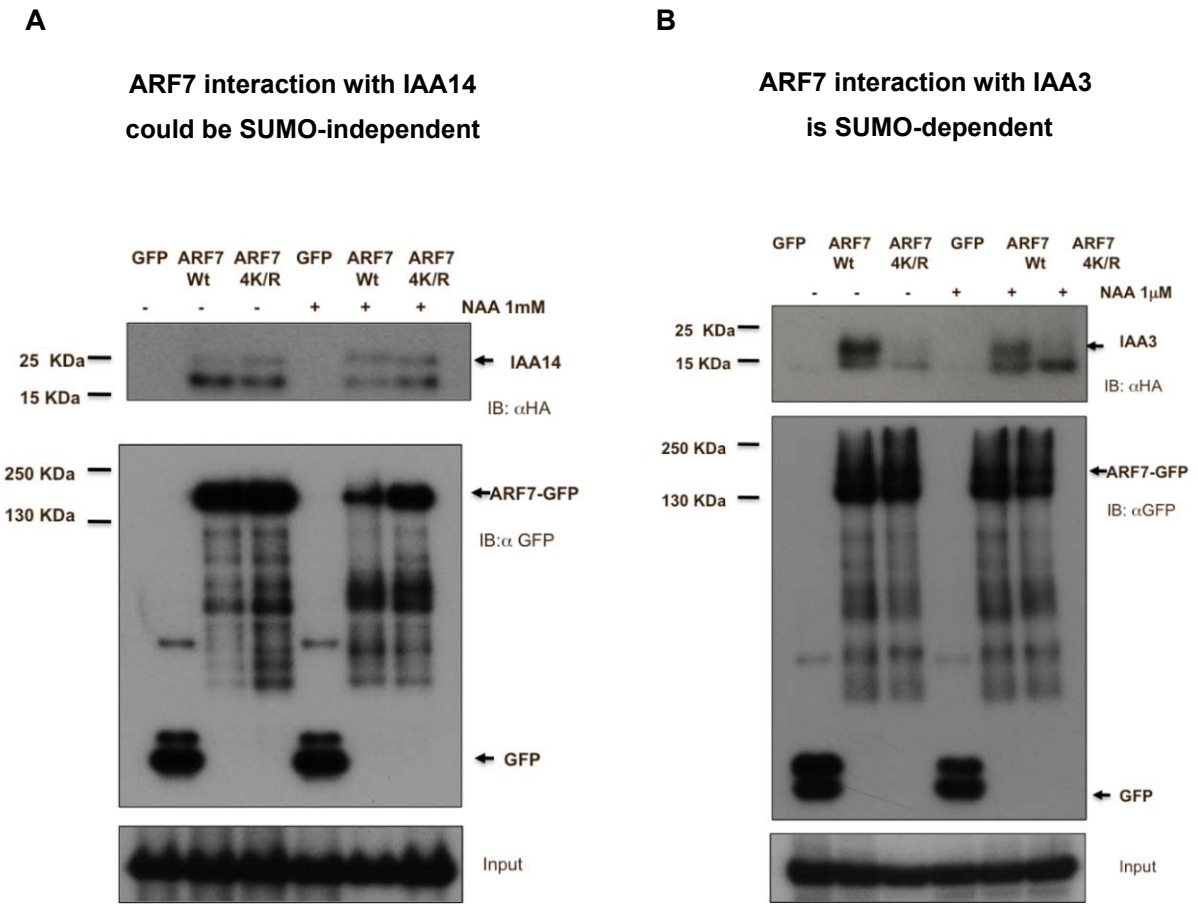

Fig. S18. ARF7 interacts with IAA3 and IAA14 in SUMO-dependent and independent manners

(**A**) ARF7-GFP and ARF7–GFP (4K/R) can interact with IAA14/SLR-HA. Transient expression was performed in *Nicotiana benthamiana* leaves using GFP, ARF7-GFP or ARF7–GFP (4K/R) with IAA14/SLR-HA treated ± 5 μM NAA for 30 min. Co-immunoprecipitation experiments were performed using GFP, ARF7-GFP or ARF7–GFP (4K/R) with IAA14/SLR-HA. Total protein (input) was subjected to immunoprecipitation with anti-GFP immunoaffinity beads followed by immunoblot analysis with anti-HA antibodies to detect IAA14/SLR-HA and anti-GFP antibodies to detect ARF7-GFP. (**B**) Only SUMOylatable ARF7-GFP interacts with IAA3/SHY2-HA. Transient expression was performed in *Nicotiana benthamiana* leaves using GFP, ARF7-GFP or ARF7–GFP (4K/R) with IAA14/SLR-HA treated ± 5 μM NAA for 30 min. Co-immunoprecipitation experiments were performed using GFP, ARF7-GFP or ARF7–GFP (4K/R) with IAA3/SHY2-HA.

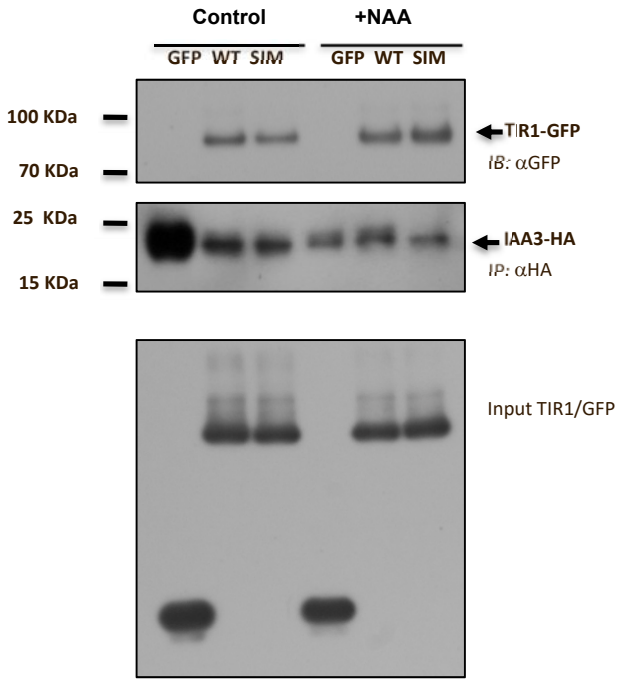

Fig. S19. IAA3/SHY2-HA lacking a SIM site remains able to interact with TIR1

Co-immunoprecipitation experiments were performed on IAA3/SHY2-HA (WT) or IAA3/SHY2-HA (SIM mutant) with TIR-GFP or GFP control. Transient assays in *Nicotiana benthamiana* leaves either co-expressing IAA3/SHY2-HA (WT) or IAA3/SHY2-HA (SIM mutant) with TIR1-GFP. Total TIR1-GFP and GFP proteins (input) were subjected to immunoprecipitation with anti-HA immunoaffinity beads followed by immunoblot analysis with anti-GFP antibodies to detect TIR-GFP and anti-HA antibodies to detect IAA3/SHY2-HA WT or IAA3/SHY2-HA SIM mutant.

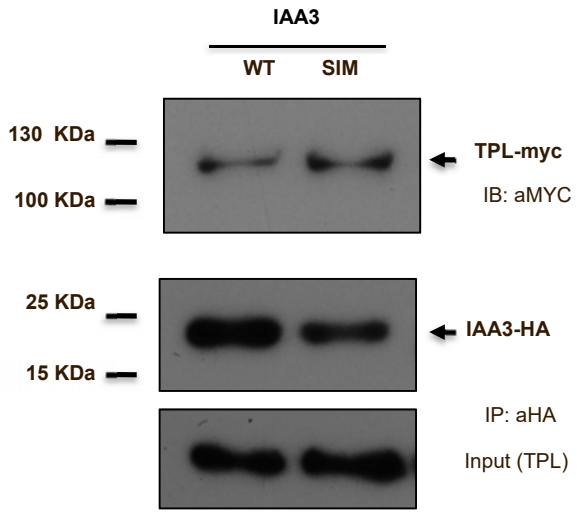

Fig. S20. IAA3/SHY2-HA lacking a SIM site remains able to interact with TOPLESS (TPL).

Co-immunoprecipitation experiments were performed on IAA3/SHY2-HA WT or IAA3/SHY2-HA SIM mutant and TPL. Transient assays were performed in *Nicotiana benthamiana* leaves either co-expressing IAA3/SHY2-HA (WT) or IAA3/SHY2-HA (SIM mutant) with TPL-Myc. Total TPL proteins (input) were subjected to immunoprecipitation with anti-HA immunoaffinity beads followed by immunoblot analysis with anti-Myc antibodies to detect TPL-Myc and anti-HA antibodies to detect IAA3/SHY2-HA WT or IAA3/SHY2-HA SIM mutant.

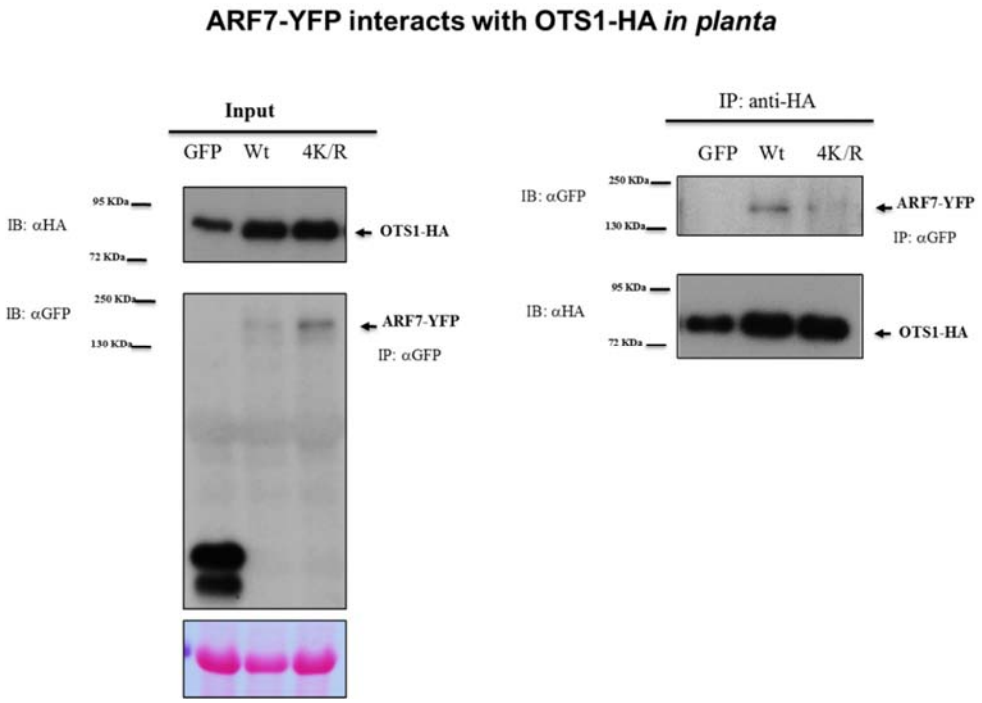

Fig. S21. OTS1 Interacts with ARF7-GFP.

Co-immunoprecipitation experiments were performed on GFP, ARF7-GFP or ARF7–GFP (4K/R) with OTS1-HA. Transient assays were performed in *Nicotiana benthamiana* leaves co-expressing either ARF7-GFP, ARF7–GFP (4K/R) or GFP with OTS1-HA. Total OTS1-HA proteins (input) were subjected to immunoprecipitation with anti-HA immunoaffinity beads followed by immunoblot analysis with anti-HA antibodies and anti-GFP antibodies.

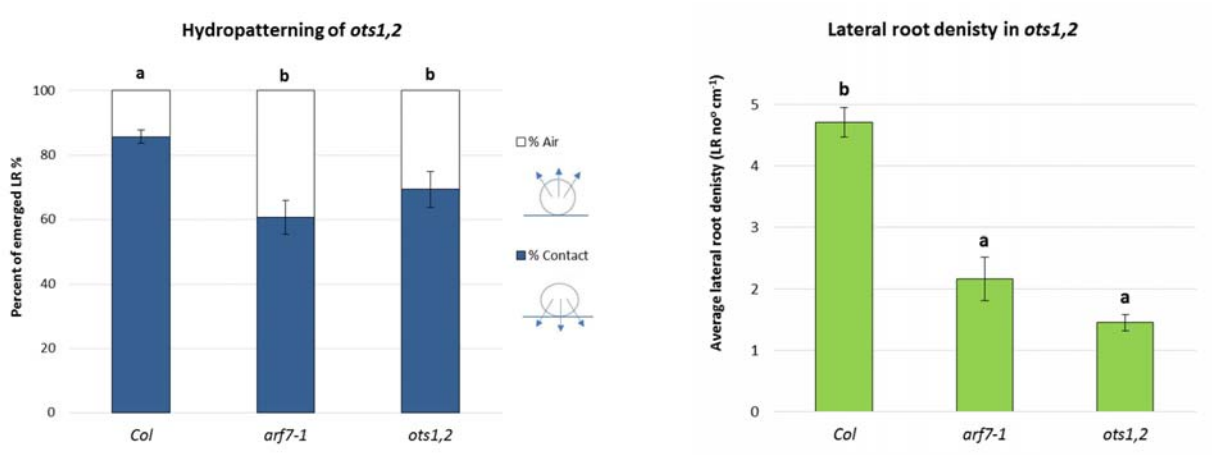

Fig. S22. Hydropatterning is dependent on *OTS1* and *OTS2*.

WT (Col-0) *Arabidopsis thaliana* roots exhibited a LR hydropatterning response that was disrupted by *ots1 ots2* and *arf7-1* mutant alleles. Data shown is mean values ± S. E. Statistical differences were analyzed on the percent of emerged LRs emerging towards either contact or air using an Anova, Tukey HSD test (P<0.05); statistically similar groups are indicated using the same letter. The independent experiment shown above feature WT >70% and *arf7-1* <60% contact, as the positive and negative controls, n LR=287/131/41 n Plants=13/12/9.

Genes	Gene Constructs	Background Vectors	Experiments
ARF7	ARF-GFP	pEG103	Co-IP
ARF7 $^{4K/R}$	ARF7$^{4K/R}$-GFP	pEG103	Co-IP
IAA3	HA-IAA3	pEG201	Co-IP
IAA3 SIM	HA-IAA3 SIM	pEG201	Co-IP
IAA14	HA-IAA14	pEG201	Co-IP
OTS1	HA-OTS1	pEG201	Co-IP
pCASP:: *shy2-2*	Shy2-2	Vermeer *et al*. 2014	Generation of transgenic plants
pCASP: :*shy2-2 SIM*	Shy2-2 SIM		Generation of transgenic plants
TIR1	GFP-TIR1	pE104	Co-IP
TPL	TPL-Myc	pGWB17	Co-IP
SUMO1	HA-SUMO	pEG201	Co-IP

Table. S1. Gateway constructs.
Constructs generated by Gateway recombination cloning technologies for Co-IP studies.

Gene	Forward Primer	Reverse Primer	Function
proARF7	ATGAAACTCAGAACCAACCA	GATCACTCAACTTTACTTTCTCTGAA	Cloning into Gateway vector
ARF7	CACCATGAAAGCTC CTTCATC	CCGGTTAAACGAAGTGGCTGAG	Cloning into Gateway vector
35S ARF7	GATGGTTAGAGAGGCTTACGC	GCTGGAGGCAACGAAATCA	Cloning into Gateway vector
ARF7 Myc	CTTGACGGTGATTCCAGG	GTTCACCGTTCAAATCTTCTT	Cloning into Gateway vector
IAA3	CACCATGGATGAGT TTGTTAACCT	TCATACACCACAGCCTAAAC	Cloning into Gateway vector
IAA14	CACCATGAACCTTAAGGAGACGGAG	TCATGATCTGTTCTTGAACTTCTCC	Cloning into Gateway vector
OTS1	CACCATGACGAAGAGGAAGAAGGA	CTCTGTCTGGTCACTGACACG	Cloning into Gateway vector
TPL	CACCATGTCTTCTCTTAGTAGAGAG	TCTCTGAGGCTGATCAGATGCAG	Cloning into Gateway vector
TIR1	CACCATGCAGAAGCGAATAGCCTTG	TTATAATCCGTTAGTAGTAATGAT	Cloning into Gateway vector
SUMO1	CACC ATGTCTGCAA ACCAGGAGGA	TCAGGCCGTAGCACCACCA	site-directed mutagenesis
ARF7 K104R	GTAAACAGATATGACAGAGATGC	GCATCTCTGTCATATCTGTTTAC	site-directed mutagenesis
ARF7 K151R	GAGCTGCTGAGAgAATCTTTCCTG	CAGGAAAGATTcTCTCAGCAGCTC	site-directed mutagenesis
ARF7 K282R	TTAGCCAgGTATACCAAAGC	GCTTTGGTATACcTGGCTAA	site-directed mutagenesis
ARF7 K889R	GATCTTTACAGCAggTCCGATATG	CATATCGGAccTGCTGTAAAGATC	site-directed mutagenesis
IAA3 SIM	CAAGGAATCTATGCGAAAGTAAGT ATG	CATACTTACTTTCGCATAGATTCC TTG	site-directed mutagenesis
TUB3	TGCATTGGTACACAGGTGAGGGAA	AGCCGTTGCATCTTGGTATTGCTG	CHIP-Q-PCR
LBD29	AGATGGTCTCTGGAAGGGTAGGTT	GCATAGTAGAACAGAATGGACGTG	CHIP-Q-PCR
LBD16	AGAAGTCTCATGTTGCAGTCTCC	TTATCGAGTGAGCCAAAGGGTGTG	CHIP-Q-PCR
CBP20	TCGTAAGGTGGGCCATGAAA	CTGATAGCTTTGCTTGCTCCTTG	Q-PCR
IAA19	TTTCCGTGGCATCGGTGTG	GCGAGCATCCAGTCTCCATC	Q-PCR
LBD29	GAGCTAGCAATGCTTCTAAG	CCAAGTCAGAGTAGATGGAG	Q-PCR
ACT7	CCATCGCTCATCGGAATGGA	TGGAACCACCACTGAGAACG	Q-PCR
LBD16 (-1021)	AGAAGTCTCATGTTGCAGTCTCC		CHIP-PCR
LBD16 (-921)	TTATCGAGTGAGCCAAAGGGTGTG		CHIP-PCR
TUB4 (-1063)	TCTCTAAGCTCTTTGGTCGCGTGT		CHIP-PCR
TUB4 (-839)	TCTTCCTCTTCCGCCTCCAACTTT		CHIP-PCR

Table. S2. Primer List.
Variety of primers used for site-directed mutagenesis, Gateway recombination cloning technology, ChIP and qPCR.

LBD16 Fold Enrichment	Control	Control	Control	Control	Control	Control	NAA 30min	NAA 30min	NAA 30min	NAA 30min	NAA 30min
arf7	1	1	1	1	1		1	1	1	1	1
pARF7 Wt	18.34	18.82	20.23	6.73	13.36		30.34	41.15	15.82	50.32	17.61
pARF7 4K/R		59.59	24.73	33.96	23.48	38.54	74.28	67.23	66.76	37.07	

ANOVA summary
F 22.64
P value < 0.0001
P value summary ****
R square 0.8251

Table S3. Data from Figure S16, ChIP-PCR assays

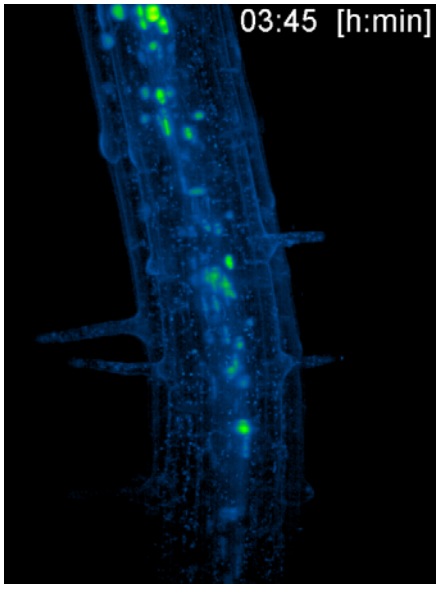

Movie S1. ***LBD16::LBD16-GFP***

Light sheet fluorescence microscopy recording of a seven days old *Arabidopsis thaliana* root expressing *LBD16::LBD16-GFP*. Maximum intensity projections of image stacks were generated from a time series with an imaging interval of 15 min.

Supplemental References

References

1. A. Hodge, The plastic plant: root responses to heterogeneous supplies of nutrients. *New Phytol.* **162**, 9–24 (2004).
2. B. D. Gruber, R. F. H. Giehl, S. Friedel, N. von Wirén, Plasticity of the Arabidopsis Root System under Nutrient Deficiencies. *Plant Physiol.* **163**, 161–179 (2013).
3. E. C. Morris *et al.*, Shaping 3D Root System Architecture. *Curr. Biol.* **27** (2017).
4. Y. Bao *et al.*, Plant roots use a patterning mechanism to position lateral root branches toward available water. *Proc. Natl. Acad. Sci. U. S. A.* **111**, 9319–24 (2014).
5. N. E. Robbins, J. R. Dinneny, Growth is required for perception of water availability to pattern root branches in plants. *Proc. Natl. Acad. Sci. U. S. A.* **115**, E822–E831 (2018).
6. J. Lavenus *et al.*, Lateral root development in Arabidopsis: fifty shades of auxin. *Trends Plant Sci.* **18**, 450–458 (2013).
7. T. Ulmasov, J. Murfett, G. Hagen, T. J. Guilfoyle, Aux/IAA proteins repress expression of reporter genes containing natural and highly active synthetic auxin response elements. *Plant Cell*. **9**, 1963–71 (1997).
8. R. Harper *et al.*, The NPH4 locus encodes the auxin response factor ARF7, a conditional regulator of differential growth in aerial Arabidopsis tissue. *Plant Cell*. **12**, 757–770 (2000).
9. Y. Okushima *et al.*, Functional Genomic Analysis of the AUXIN RESPONSE FACTOR Gene Family Members in Arabidopsis thaliana: Unique and Overlapping Functions of ARF7 and ARF19. *Plant Cell*. **17**, 444–463 (2005).
10. M. A. Moreno-Risueno *et al.*, Oscillating Gene Expression Determines Competence for Periodic Arabidopsis Root Branching. *Science (80-.).* **329**, 1306–1311 (2010).
11. B. Péret *et al.*, Auxin regulates aquaporin function to facilitate lateral root emergence. *Nat. Cell Biol.* **14**, 991–998 (2012).
12. J. Lavenus *et al.*, Inference of the Arabidopsis Lateral Root Gene Regulatory Network Suggests a Bifurcation Mechanism That Defines Primordia Flanking and Central Zones. *Plant Cell*. **27**, 1368–1388 (2015).
13. T. Goh *et al.*, Quiescent center initiation in the Arabidopsis lateral root primordia is dependent on the SCARECROW transcription factor. *Development*. **143**, 3363–71 (2016).
14. E. S. Johnson, Protein Modification by SUMO. *Annu. Rev. Biochem.* **73**, 355–382 (2004).
15. D. R. Boer *et al.*, Structural basis for DNA binding specificity by the auxin-dependent ARF transcription factors. *Cell*. **156**, 577–89 (2014).
16. T. Goh, H. Kasahara, T. Mimura, Y. Kamiya, H. Fukaki, Multiple AUX/IAA-ARF modules regulate lateral root formation: the role of Arabidopsis SHY2/IAA3-mediated auxin signalling. *Philos. Trans. R. Soc. Lond. B. Biol. Sci.* **367**, 1461–8 (2012).
17. K. Swarup *et al.*, The auxin influx carrier LAX3 promotes lateral root emergence. *Nat. Cell Biol.* **10**, 946–954 (2008).
18. J. E. M. Vermeer *et al.*, A spatial accommodation by neighboring cells is required for organ initiation in arabidopsis. *Science (80-.).* **343** (2014).
19. L. Conti *et al.*, Small Ubiquitin-like Modifier Protein SUMO Enables Plants to Control

Growth Independently of the Phytohormone Gibberellin. *Dev. Cell*. **28**, 102–110 (2014).
20. L. Conti *et al.*, Small ubiquitin-like modifier proteases OVERLY TOLERANT TO SALT1 and -2 regulate salt stress responses in Arabidopsis. *Plant Cell*. **20**, 2894–908 (2008).
21. T. Nakagawa *et al.*, Improved Gateway Binary Vectors: High-Performance Vectors for Creation of Fusion Constructs in Transgenic Analysis of Plants, doi:10.1271/bbb.70216.
22. S. J. Clough, A. F. Bent, Floral dip: a simplified method for Agrobacterium-mediated transformation of Arabidopsis thaliana. *Plant J.* **16**, 735–43 (1998).
23. M. M. Goodin, R. G. Dietzgen, D. Schichnes, S. Ruzin, A. O. Jackson, pGD vectors: versatile tools for the expression of green and red fluorescent protein fusions in agroinfiltrated plant leaves. *Plant J.* **31**, 375–383 (2002).
24. J. D. Nelson, O. Denisenko, P. Sova, K. Bomsztyk, Fast chromatin immunoprecipitation assay. *Nucleic Acids Res.* **34**, e2 (2006).
25. H. Cho *et al.*, A secreted peptide acts on BIN2-mediated phosphorylation of ARFs to potentiate auxin response during lateral root development. *Nat. Cell Biol.* **16**, 66–76 (2014).
26. D. von Wangenheim, R. Hauschild, J. Friml, Light sheet fluorescence microscopy of plant roots growing on the surface of a gel. *J. Vis. Exp.* **2017** (2017).
27. S. Preibisch *et al.*, Efficient Bayesian-based multiview deconvolution. *Nat. Methods*. **11**, 645–648 (2014).
28. S. Preibisch, S. Saalfeld, J. Schindelin, P. Tomancak, Software for bead-based registration of selective plane illumination microscopy data. *Nat. Methods*. **7**, 418–419 (2010).